Quaternary Science Reviews 246 (2020) 106517

Contents lists available at ScienceDirect

Quaternary Science Reviews

journal homepage: www.elsevier.com/locate/quascirev

Sub-millennial eruptive recurrence in the silicic Mangaone Subgroup tephra sequence, New Zealand, from Bayesian modelling of zircon double-dating and radiocarbon ages

Martin Danišík [a, *], David J. Lowe [b], Axel K. Schmitt [c], Bjarne Friedrichs [c], Alan G. Hogg [b], Noreen J. Evans [a]

[a] John de Laeter Centre/School of Earth and Planetary Sciences, Curtin University, Perth, WA 6845, Australia
[b] School of Science, University of Waikato, Private Bag 3105, Hamilton, 3240, New Zealand
[c] Institute of Earth Sciences, Ruprecht-Karls-Universität Heidelberg, Im Neuenheimer Feld 236, D-69120, Heidelberg, Germany

ARTICLE INFO

Article history:
Received 11 June 2020
Received in revised form
20 July 2020
Accepted 24 July 2020
Available online xxx

Keywords:
Zircon double-dating
(U–Th)/He
U–Th disequilibrium
Radiocarbon dating
Bayesian age sequence modelling
Magma dynamics
Mangaone Subgroup
Tephrochronology
Okataina Volcanic Centre
Taupo Volcanic Zone

ABSTRACT

Accurate dating of young (<1 Ma) volcanic eruptions has long been a challenge for modern geochronology given the scarcity of datable mineral phases and low quantities of radiogenic daughter products. Combined U–Th–Pb and (U–Th)/He dating of zircon (i.e., zircon double-dating, ZDD) is a relatively new dating approach that offers a viable option for dating zircon-bearing volcanic and pyroclastic deposits as young as ca. 3 ka, and has a great potential for application in many fields within the Quaternary sciences, including volcanology, palaeoclimatology, and archaeology. In our study, a stratigraphically and spatially well-defined sequence of 13 rhyodacitic to rhyolitic tephra beds – the Mangaone Subgroup (MSg) – erupted from the Okataina Volcanic Centre (OVC), is used as a natural laboratory to conduct a cross-validation experiment in which the ZDD eruption ages are compared with published and new radiocarbon (^{14}C) eruption ages. These ZDD and ^{14}C ages are then used together to underpin a Bayesian age model developed (using ChronoModel) to provide new ages for the entire MSg sequence. New ZDD eruption ages of 36.1 ± 4.4, 31.5 ± 5.2, 30.9 ± 5.6, 31.2 ± 4.4 ka BP for four MSg tephras (Units D, I, J, and K, respectively) are statistically indistinguishable from ^{14}C-based eruption ages. These results validate the feasibility of ZDD to date late Quaternary eruptions accurately. The Bayesian age sequence model provides provides an eruptive geochronology eruptive geochronology for all 13 MSg tephra beds for the first time (and for the stratigraphically-interbedded Taupo-volcano-derived Tahuna tephra, $38.4^{+1.7}_{-1.4}$ ka BP), and constrains the beginning of the MSg eruption period to $42.7^{+3.7}_{-3.5}$ ka BP (Unit A) and the end to $30.6^{+0.6}_{-1.5}$ ka BP (Unit L). Thus, the entire MSg sequence was emplaced in ~12,100 years, representing an eruption frequency of one event per ~930 years on average. Our study demonstrates the efficacy of ZDD to yield accurate eruption ages on pyroclastic deposits, highlighting its potential for dating young (<1 Ma) magmatic and eruption events that are difficult to date by other geochronological methods, and also shows that ZDD dates can be integrated with ^{14}C ages using Bayesian modelling to develop new age models for long sequences of tephra beds, in this case those of the MSg tephras that were deposited during MIS 3. In addition, the U–Th zircon crystallization data revealed distinct U–Th model age spectra for older and younger MSg tephras, providing geochronological evidence for a decreasing degree of interconnectedness within the OVC magma reservoir during the MSg eruption period that followed caldera collapse associated with the pre-MSg Rotoiti (Rotoehu) eruption at ca. 45 ka BP.

1. Introduction

Accurate dating of young (<1 Ma) geological materials is of paramount importance to Quaternary science, yet this time interval arguably presents one of the major technical challenges for modern

* Corresponding author. Low-Temperature Thermochronology Facility, John de Laeter Centre, Curtin University, Perth, WA 6845, Australia.
E-mail address: m.danisik@curtin.edu.au (M. Danišík).

https://doi.org/10.1016/j.quascirev.2020.106517
0277-3791/

geochronology. Young volcanic eruptions are chiefly dated by high-precision techniques such as radiocarbon (^{14}C) and ^{40}Ar/^{39}Ar on sanidine (e.g., Mark et al., 2017; Hogg et al., 2019). Combined U–Th–Pb and (U–Th)/He dating of zircon (a.k.a. zircon double-dating or ZDD; Danišík et al., 2017a), with an applicability range from 1 Ma to ~3 ka (Schmitt et al., 2012; Danišík et al., 2017a; Kirkland et al., 2020), is a relatively new dating method (Schmitt et al., 2006, 2010b) that offers a viable option.

ZDD principles and analytical procedures have been summarized in detail by Danišík et al. (2017a). In brief, ZDD is based on 'dependent' determination of two distinct ages on a single zircon crystal: crystallization ages are first determined via U–Pb or U–Th disequilibrium geochronology; these ages are robust crystallization ages even under magmatic conditions (Cherniak and Watson, 2001). To preserve crystal volume, high spatial resolution methods with low material consumption are used, such as secondary ionisation mass spectrometry (SIMS) (Fig. 1) (Schmitt et al., 2006; Schmitt, 2007, 2011) or laser ablation inductively coupled plasma mass-spectrometry (LA-ICPMS) (Ito and Danišík, 2020). Cooling ages of U–Th–Pb dated crystals are then determined via (U–Th)/He thermochronometry (T_c < 300 °C; Reiners et al., 2004). For crystals with a cooling age <1 Ma, (U–Th)/He data may require correction for disequilibrium in the U and Th decay chains (Farley et al., 2002). The magnitude of the disequilibrium correction depends on pre-eruptive residence time and is determined on a crystal-by-crystal basis from the crystallization and cooling age pairs (Schmitt et al., 2010b). Finally, disequilibrium-corrected (U–Th)/He ages, which are typically determined on replicate crystals per sample, are used to calculate a representative mean value for the population, interpreted as the eruption age (hereafter referred to as ZDD eruption age).

Precision on ZDD eruption ages is typically 5–12% at the 2σ level, which is relatively low compared to high-precision ^{14}C or sanidine ^{40}Ar/^{39}Ar data, commonly reported with 2σ uncertainties of <2%. Nevertheless, the ZDD has tremendous potential for Quaternary geochronology as it covers the critical 1 Ma to ca. 50 ka time window, which is beyond the reach of the ^{14}C method (≤50 ka under most circumstances; Hogg et al., 2007) and difficult to access using other techniques. In fact, ZDD may often be the only tool applicable to dating intermediate to silicic calc-alkaline volcanic rocks or pyroclastic deposits typical of subduction zones. These materials have been notoriously challenging to date using the K–Ar and ^{40}Ar/^{39}Ar methods due to their low potassium content and the frequent absence of K-rich phases, but they commonly contain zircon. Indeed, during the past five years, ZDD has been increasingly applied in tephrostratigraphy, volcanic and magmatic geochronology, and occasionally even in archaeology and paleoanthropology (e.g., Coble et al., 2017; Mucek et al., 2017; Molnár et al., 2018; Burgess et al., 2019; Ulusoy et al., 2019; Sisson et al., 2019; Gençalioğlu-Kuşcu et al., 2020).

Several studies report demonstrably accurate ZDD eruption ages, in agreement with independent geochronological constraints obtained by dating co-genetic mineral phases or bracketing units (e.g., Schmitt et al., 2010a, b; Danišík et al., 2012; Harangi et al., 2015; Ito and Danišík, 2020). Moreover, ZDD has a unique built-in consistency check because the eruption age has to postdate the zircon crystallization age. However, as with any geochronological method, maintaining a level of scepticism about reliability of the age relevance of ZDD results is warranted, in particular when ZDD ages are not entirely concordant with long accepted ages derived using more established methods (e.g., Wilson and Rowland, 2016; Hopkins et al., 2017; Chesner et al., 2020). U–Th–Pb and (U–Th)/He dating procedures are usually vetted against secondary reference materials (e.g., AS3 and 91500 zircons for U–Th–Pb and Fish Canyon zircon for (U–Th)/He); however, a suitable reference material that can be used to monitor the accuracy of the coupled ZDD

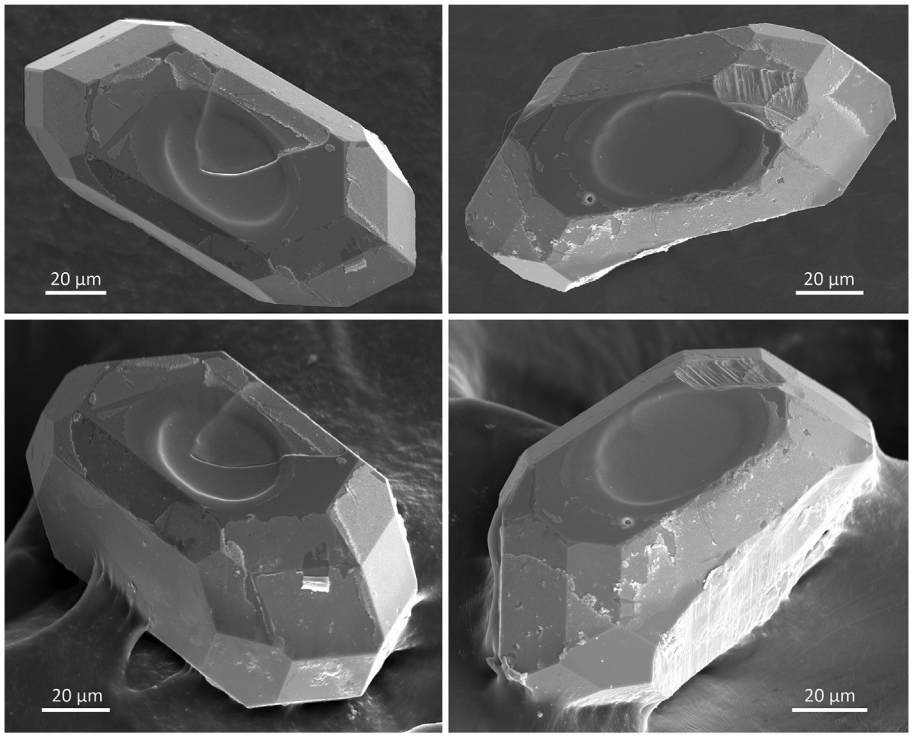

Fig. 1. Secondary electron images of two zircon crystals (top panels – planar view; bottom panels – perspective view) after SIMS analysis showing the minimal material consumption of CAMECA ims 1280-HR required for U–Th analysis. Sputtered elliptical craters are 40 × 25 μm in length and width, respectively, and 4 μm deep, and so the majority of the crystal remains intact for subsequent (U–Th)/He analysis.

approach has not yet been developed. Ideally, this standard would be a well characterized, widely available zircon with an accurately and precisely known crystallization and eruption age of <350 ka (for the U–Th + (U–Th)/He dating combination) or <1 Ma (for the U–Pb + (U–Th)/He) dating combination). Secondly, verification of ZDD eruption ages against independent constraints is only rarely possible in nature due to the scarcity of truly co-genetic minerals or other materials in volcanic deposits that are datable by independent geochronological methods. Lastly, with the exception of studies by Schmitt et al. (2012) and Danišík et al. (2012), the accuracy of ZDD has not been rigorously tested. Therefore, there is a need for further cross-validation studies that compare ZDD results with independent dating techniques.

This work describes such a cross-validation experiment in which we target a stratigraphically and spatially well-defined sequence of Mangaone Subgroup tephras from New Zealand's North Island (Vucetich and Pullar, 1969; Howorth, 1975). The Mangaone Subgroup (MSg) tephra beds represent the products of 13 primarily rhyolitic eruption episodes at the Okataina Volcanic Centre (OVC), within the central Taupo Volcanic Zone (Fig. 2), that occurred between about 50 and 25 ka (Jurado-Chichay and Walker, 2000, 2001a; Smith et al., 2002, 2005). This period is entirely within Marine Isotope Stage 3 (e.g., Wright et al., 1995; Wilson et al., 2007; Siddall et al., 2008). Some of the MSg tephras have been extensively dated by ^{14}C methods (34 published dates since 1969) and so the general timeframe of their eruptive history is now established (Froggatt and Lowe, 1990; Jurado-Chichay and Walker, 2000; Shane et al., 2006; Molloy et al., 2009). However, around half of the 13 beds in the sequence have never been dated directly. The tephras are silicic in composition (see Section 2) and some contain zircon (Charlier and Wilson, 2010). They are well exposed, regionally widespread (including in marine cores), and their stratigraphic framework has been established in detail (Howorth, 1975; Jurado-Chichay and Walker, 2000; Nairn, 2002; Smith et al., 2002; Shane et al., 2006; Wilson et al., 2009). Cumulatively, these attributes make the MSg an excellent natural laboratory in which to test the accuracy of ZDD against eruption ages derived from the ^{14}C method.

Accordingly, we report here ZDD eruption ages for some MSg tephras, complemented with new ^{14}C ages. Our results demonstrate the capability of the ZDD approach to yield accurate eruption ages. In addition to the new geochronological data, we present a new Bayesian age sequence model combining both the ZDD and ^{14}C data with stratigraphic constraints, and reconstruct an eruptive chronology for the entire Mangaone Subgroup, the first time such a modelling approach has been used for the sequence. In doing so, we provide new modelled ages for the beginning (Unit A) and end (Unit L) of the MSg tephra sequence. Finally, we assess the implications of new ZDD data for OVC magmatic dynamics.

2. Mangaone Subgroup

2.1. Volcanologic and compositional context

The Mangaone Subgroup (MSg) is a sequence of 13 silicic plinian and phreatoplinian pyroclastic deposits (tephras) that originated from the OVC (which lies in the northeast part of the central Taupo Volcanic Zone) (Jurado-Chichay and Walker, 2000; Smith et al., 2002). The MSg beds are stratigraphically bracketed by (i) deposits of the underlying Rotoiti Tephra Formation (which formally comprises three members: Matahi Scoria, from basaltic fallout; the non-welded Rotoiti Ignimbrite, from rhyolitic pyroclastic flows (density currents); and the Rotoehu Ash, from rhyolitic fallout: Froggatt and Lowe, 1990) (45.2 ± 3.3 ka (2σ); Danišík et al., 2012); and (ii) the overlying Kawakawa/Oruanui tephra (25.4 ± 0.2 cal ka (2σ); Vandergoes et al., 2013). The two voluminous and widespread rhyolitic members of the Rotoiti Tephra are correlatives and are of the same age (Nairn, 1972), hence are used interchangeably in this paper as appropriate. (The Matahi Scoria is a minor component and not present in the sampling area and hence is not considered further.)

The MSg volcanic episode represents a period of intra-caldera modification in the OVC, which followed the caldera-forming Rotoiti eruption (ca. 45 ka) and preceded a period of caldera infilling and dome-building starting at ca. 21 ka (Nairn, 1989; Cole et al., 2010, 2014). Eruptions were typically relatively small- to medium-sized (non-consolidated volumes: 0.4–19.9 km^3; minimum total bulk volume: 80.7 km^3; Table 1), short-lived (<12 h), and closely spaced plinian-type, resulting in extensive pumice-rich

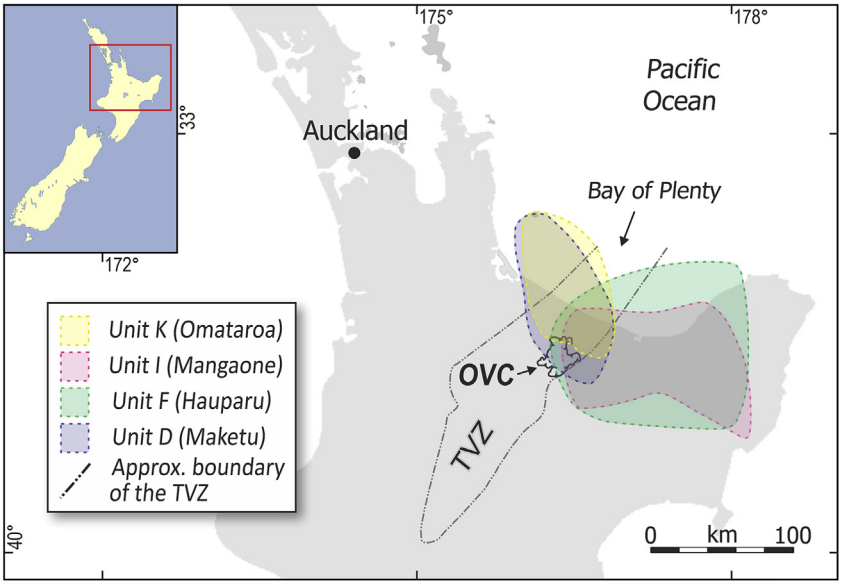

Fig. 2. Distribution of the most widespread MSg tephras in the North Island of New Zealand (modified after Jurado-Chichay and Walker, 2000). OVC – Okataina Volcanic Centre; TVZ – Taupo Volcanic Zone, simplified boundary after Wilson et al. (2009). *Inset:* Location map, New Zealand.

Table 1
Summary of stratigraphy, nomenclature and volume for MSg tephras.[a,b]

Howorth (1975)	Jurado-Chichay and Walker (2000)	Smith et al. (2002)		Smith et al. (2005)	Wilson et al. (2009)	This study	Volume (km^3)[a]
Omataroa	Unit L	Unit L		Unit L	Unit L (Okataina)	Unit L	8.1
	Unit K	Omataroa	Young MSg	Omataroa	Unit K (Okataina)	Unit K (Omataroa)	16.2
Awakeri	Unit J	Awakeri		Awakeri	Unit J (Okataina)	Unit J (Awakeri)	0.77
Mangaone	Unit I	Mangaone		Mangaone	Unit I (Okataina)	Unit I (Mangaone)	19.9
Hauparu	Unit H	Unit H		Unit H	Unit H (Okataina)	Unit H	0.1
	Unit G	Unit G		Unit G	Unit G (Okataina)	Unit G	2.5
	Unit F	Hauparu		Hauparu	Unit F (Okataina)	Unit F (Hauparu)	15.2
Te Mahoe	Unit E	Te Mahoe		Te Mahoe	Unit E (Okataina)	Unit E (Te Mahoe)	0.9
Maketu	Unit D	Maketu		Maketu	Unit D (Okataina)	Unit D (Maketu)	11
Tahuna[b]	*Tahuna*[b]		Old MSg				4
Ngamotu	Unit C	Pongakawa		Pongakawa	Unit C2 (Okataina)	Unit C2 (Pongakawa)	0.7
		Pupuwharau		Pupuwharau	Unit C1 (Okataina)	Unit C1 (Pupuwharau)	
		Tahuna[b]		*Tahuna*[b]	*Tahuna (Taupo)*	*Tahuna*[b]	4
	Unit B	Ngamotu		Ngamotu	Unit B (Okataina)	Unit B (Ngamotu)	4.6
	Unit A	Unit A		Unit A	Unit A (Okataina)	Unit A	0.44

[a] Non-consolidated volume after Jurado-Chichay and Walker (2000) for MSg tephras, and after Wilson et al. (2009) for Tahuna tephra.
[b] Not erupted from Okataina Volcanic Centre (Smith and Shane, 2002).

tephra beds (Jurado-Chichay and Walker, 2000, 2001a, b; Smith et al., 2005). The MSg tephras are typically separated by paleosols, usually thin, and because of their widespread occurrence, the tephras provide useful stratigraphic marker horizons for the central and northern North Island of New Zealand (Pullar et al., 1973; Hogg and McCraw, 1983; McGlone et al., 1984; Molloy et al., 2009; Hopkins et al., 2017) and offshore including the Pacific Ocean (Fig. 2) (Houghton et al., 1992; Pillans and Wright, 1992; Wright et al., 1995; Shane et al., 2006; Wilson, 2007). Compositions of MSg tephras range from rhyodacitic to rhyolitic (68–75.5 wt% SiO_2; Smith et al., 2002, 2005) and at least two contain zircon (Charlier and Wilson, 2010), providing an opportunity to apply ZDD.

2.2. Nomenclature and stratigraphy

Different nomenclatures have been used interchangeably in the literature to describe the MSg tephra beds, which may be confusing to readers unfamiliar with New Zealand tephrostratigraphy. We therefore provide a short review of MSg terminology and stratigraphy as they are currently understood.

The MSg sequence was first referred to as the 'Mangaoni Lapilli Formation' by Vucetich and Pullar (1969). The authors used the term to describe a distinct package of shower-bedded pumice lapilli and blocks-and-ash beds, bracketed by the Rotoehu Ash (below) and Oruanui Formation (above). Five deposits were recognized (units *a*–*e*) within the formation (Vucetich and Pullar, 1969). The name of the sequence was changed to 'Mangaone Subgroup', as proposed by Howorth (1981), and later formalized by Froggatt and Lowe (1990) (the use of 'Mangaone' rather than 'Mangaoni' by Howorth in 1975 corrected a spelling error on a topographic map). The MSg tephra beds were defined as originating from the OVC (Froggatt and Lowe, 1990). Cole et al. (2010, 2014) employed the alternative term 'Mangaone Pyroclastic Subgroup'. A detailed stratigraphy of the sequence was first constructed by Howorth (1975), who described eight tephra formations and defined them using local geographic names that have since been widely accepted. In ascending stratigraphic order, these formations are Ngamotu, Tahuna, Maketu, Te Mahoe, Hauparu, Mangaone, Awakeri, and Omataroa (Table 1). Note that the subgroup's collective name (Mangaone) is also used as the name of one of the constituent tephra formations.

The MSg stratigraphy was later revised by Jurado-Chichay and Walker (2000) and Smith et al. (2002) who described 12 and 14 tephra deposits, respectively, and named these with letters (Units A–L; Jurado-Chichay and Walker, 2000) or a combination of letters and local names (Smith et al., 2002) (Table 1). Smith and Shane (2002) demonstrated that the Tahuna tephra did not erupt from the OVC and therefore should not be a member of the Mangaone Subgroup (although it is present in the MSg sequence at many sites). Further changes to the nomenclature have been made by Smith et al. (2005) who subdivided the MSg based on age and composition into 'Old MSg' (Units A-G; ~40–35 ka; low-SiO_2 rhyodacite) and 'Young MSg' (Units H-L; ~35–31.5 ka; high-SiO_2 rhyolite) episodes, and by Wilson et al. (2009) who introduced Units C1 and C2 as a compromise between Unit C *sensu* Jurado-Chichay and Walker (2000) and Pupuwharau and Pongakawa tephras *sensu* Smith et al. (2002) (Table 1).

The name 'Kawerau Ignimbrite' has been applied to the most voluminous and extensive of the MSg eruptives, Unit I (Mangaone tephra), the eruption of which may have been accompanied by partial caldera collapse (Cole et al., 2010, 2014). These authors indicate that this non-welded ignimbrite is associated geochemically with the younger of the two MSg magma types noted above (Smith et al., 2002). The term 'Kawerau' has not been widely adopted, partly because of confusion regarding its age when first reported, and partly because the ignimbrite had already been

Table 2
Summary of ^{14}C data.

Unit/Sample ID	Material dated	Source[a]	Conventional ^{14}C age (yr BP)[b]	±1σ (yr)	Calibrated ^{14}C age[c] (cal yr BP)	Calibrated 1σ age range (cal yr BP)	Calibrated 2σ age range (cal yr BP)	Models[d] 1, 2	Model[d] 3
Unit L									
L1	charcoal	6	26,520	220	30,746	30,585–30,956	30,291–31,088	x	x
Unit K (Omataroa)									
O1	charcoal	1	27,900	850	32,069	31,110–32,815	30,675–33,890	x	x
O2	organic mud	2	29,700	1500	33,943	31,912–35,276	31,084–38,001	x	x
O3	organic mud	2	27,900	1200	32,183	30,980–33,330	29,777–34,741	x	x
Pooled samples									
O1-3		5	28,220	315	32,085	31,566–32,480	31,331–32,970		
O1-3, L1		7	26,700	1988	31,309	28,839–33,275	27,415–37,271		
O1-3		10			32,322	31,476–32,926	31,165–33,674		
Unit I (Mangaone)									
BDQ-1a (Wk-42097a)	charcoal	10	26,846	117	30,958	30,858–31,060	30,752–31,150	x	x
BDQ-1b (Wk-42097b)	charcoal	10	26,892	117	30,981	30,883–31,082	30,777–31,171	x	x
M1	charcoal contamin. with roots	1	26,300	700	30,363	29,717–31,024	28,868–31,564		x
M2	charcoal contamin. with roots	2	21,900	400	26,177	25,742–26,568	25,435–27,137		x
M3	charcoal	2	30,100	1300	34,290	32,766–35,687	31,433–37,684		x
M4	soil	2	29,400	800	33,416	32,560–34,313	31,547–34,966		x
M5	charcoal	4	26,100	800	30,181	29,456–30,966	28,540–31,664		x
M6	extract	4	26,800	1400	31,064	29,430–32,521	28,333–34,358		x
M7	residue	4	25,000	700	29,143	28,291–29,861	27,833–30,671		x
M8	charcoal	4	35,300	2200	40,054	37,469–42,225	35,438–45,598		x
M9	charcoal	4	31,400	1500	35,829	33,953–37,375	32,820–39,981		x
M10	peat	4	27,000	1000	31,150	29,930–32,185	29,200–33,569		x
M11	peat	4	31,000	2100	35,773	33,177–38,256	31,329–41,535		x
M12	charcoal	3	33,300	2000	37,998	35,464–39,982	34,004–42,813		x
M13	charcoal	6	27,780	270	31,538	31,225–31,770	31,095–32,357	x	x
M14	charcoal	6	28,340	270	32,202	31,734–32,601	31,456–33,003	x	x
Pooled samples									
BDQ1a, b		10			30,958	30,858–31,060	30,752–31,150		
M3-M12		5	27,730	350	31,559	31,154–31,856	31,022–32,550		
M13-14		6	28,060	270	31,863	31,425–32,193	31,276–32,693		
M3-M5, M8, M10-M14		7	28,140	3535	34,375	28,834–38,288	27,411–47,134		
M13-14; BDQ1a,b		10			31,081	30,999–31,169	30,902–31,247		
Unit F (Hauparu)									
H1	organic mud	4	39,000	5600	43,694	40,199–48,146	37,357 - [>50,000]	x	x
H2	organic mud	4	35,700	1300	40,285	39,000–41,525	37,610–42,864	x	x
Pooled samples									
H1–H2		5	35,870	1270	40,444	39,220–41,646	37,998–42,934		
		10			40,564	39,367–41,768	38,202–43,041		
Unit E (Te Mahoe)									
E1 (?)	soil between U's F and Dmost likely dating unit E	6	31,720	370	35,577	35,171–35,974	34,828–36,321	x	x
Maketu (Unit D)									
K1	bulk sediment	8	31,750	580	35,662	35,004–36,201	34,493–37,183	x	x
K2	macrofossil charcoal	8	32,200	360	36,067	35,642–36,427	35,185–36,997	x	x
Pooled samples									
K1–K2		8	32,078	306	35,933	35,614–36,259	35,215–36,590		
K1–K2		10			35,937	35,617–36,262	35,219–36,595		

(*continued on next page*)

Table 2 (*continued*)

Unit/Sample ID	Material dated	Source[a]	Conventional ^{14}C age (yr BP)[b]	±1σ (yr)	Calibrated ^{14}C age[c] (cal yr BP)	Calibrated 1σ age range (cal yr BP)	Calibrated 2σ age range (cal yr BP)	Models[d] 1, 2	Model[d] 3
Tahuna									
T1	bulk sediment	8	33,340	520	37,543	36,855–38,279	36,260–38,771	x	x
T2	macrofossil charcoal	8	34,060	470	38,486	37,879–39,106	37,047–39,655	x	x
T3	plant macrofossils	9	34,360	460	38,864	38,385–39,402	37,714–40,019	x	x
Pooled samples									
T1-T2		8	33,737	349	38,069	37,622–38,603	36,909–38,883		
T1-T3		10			38,452	38,154–38,794	37,590–39,130		

[a] 1 - Vucetich and Pullar (1969); 2 - Pullar and Heine (1971); 3 - Nairn (1981); 4 - McGlone et al. (1984); 5 - Froggatt and Lowe (1990); 6 - Jurado-Chichay and Walker (2000); 7 - Shane et al. (2006); 8 - Molloy et al. (2009); 9 - Loame et al. (2019); 10 - this study.

[b] yr BP - years before present where present = 1950 CE.

[c] Median of calibrated ^{14}C age distribution in years before the present (cal yr BP) calibrated in OxCal 4.3 software (Bronk Ramsey, 2009) using the SHCal13 calibration curve (Hogg et al., 2013).

[d] Ages used for Bayesian age sequence modelling as described in the text.

defined as the 'upper Mangaone member' of the Mangaone Tephra Formation by Howorth (1975).

In this study we followed the latest version of stratigraphy after Wilson et al. (2009) and use a 'hybrid' nomenclature combining the systems of Jurado-Chichay and Walker (2000) and Smith et al. (2002) as presented in Table 1.

2.3. Previous geochronology

Seven of the MSg tephras have been previously dated by ^{14}C methods (see the summary of ^{14}C data in Table 2 and Fig. 3). Preferred eruption ages and age precision for some tephras vary significantly, depending on data treatment. For example, 17 ^{14}C ages ranging between 26.2 ± 0.4 and 40.1 ± 2.1 cal ka BP (1σ) have been obtained for different materials from Unit I (Mangaone) (Vucetich and Pullar, 1969; Pullar and Heine, 1971; Nairn, 1981; McGlone et al., 1984; Jurado-Chichay and Walker, 2000). Representative eruption ages preferred by different authors based on the same dataset vary from 31.6 ± 0.4 to 33.0 ± 3.7 cal ka BP (1σ) depending on data selection preference (Jurado-Chichay and Walker, 2000; Shane et al., 2006). As noted by Froggatt and Lowe (1990), the assumption of high quality in the ^{14}C data is not always warranted and care needs to be taken when selecting data for interpretation. Similarly, McGlone et al. (1984) reported that radiocarbon ages obtained on MSg tephras within peat at a site in Gisborne "do not give a conclusive indication of [their] age [but] collectively they suggest that the site is between 30,000 and 40,000 years old" (p. 333).

To make the available data comparable and consistent with international standardization and nomenclature, we have calibrated conventional ^{14}C ages (in ^{14}C yr BP) to calendar years (cal yr BP or cal ka BP) in the OxCal 4.3 software (Bronk Ramsey, 2009) using the SHCal13 calibration curves (Hogg et al., 2013) (Table 2). The ^{14}C ages from, or relevant to, the MSg that we consider reliable range from 38.9 ± 0.5 (Tahuna Tephra; in Loame et al., 2019) to 30.7 ± 0.2 cal ka BP (1σ) (Unit L; Jurado-Chichay and Walker, 2000).

As noted earlier, around half of the MSg tephras have never been directly dated by radiometric methods and their ages have instead been inferred based on stratigraphic relationship and assumptions relating to the duration of paleosol formation (the amount of time it took for soil horizons to be developed prior to burial by new eruptives). Neither of the two stratigraphically oldest MSg tephras, Unit A and Unit B (Ngamotu), has been dated directly. Consequently, the beginning of the MSg eruptive phase was only indirectly estimated at ~52–43 ka based on field observations (Jurado-Chichay and Walker, 2000) made in conjunction with the widely varying estimates for the eruption age of the underlying Rotoiti eruptives (including the Rotoehu Ash) (Froggatt and Lowe, 1990). The Rotoiti/Rotoehu deposits have been very difficult to constrain chronologically, and ages have ranged from ca. 40 ka to 70 ka (e.g., Thompson, 1968; Grant-Taylor and Rafter, 1971; Berryman, 1992; Lowe and Hogg, 1995; Lian and Shane, 2000; Santos et al., 2001; Shane and Sandiford, 2003; Wilson et al., 2007; Flude and Storey, 2016). In our study, we adopt the eruption age of 45.2 ± 3.3 ka (2σ) for the Rotoiti Tephra Formation (Danišík et al., 2012) and consider it to be the maximum age limit for the MSg tephra beds. This age was derived by ZDD and evidence supporting it includes (but is not limited to) optimum ^{14}C data (i.e., stratigraphically well-constrained samples and high-level laboratory pre-treatment) (Santos et al., 2001; Danišík et al., 2012), ^{40}Ar/^{39}Ar data on K-feldspar and biotite (Flude and Storey, 2016), U–Th zircon crystallization ages (Charlier et al., 2003; Charlier and Wilson, 2010; Rubin et al., 2016), as well as palynological, magnetostratigraphic, and sedimentation-rate-

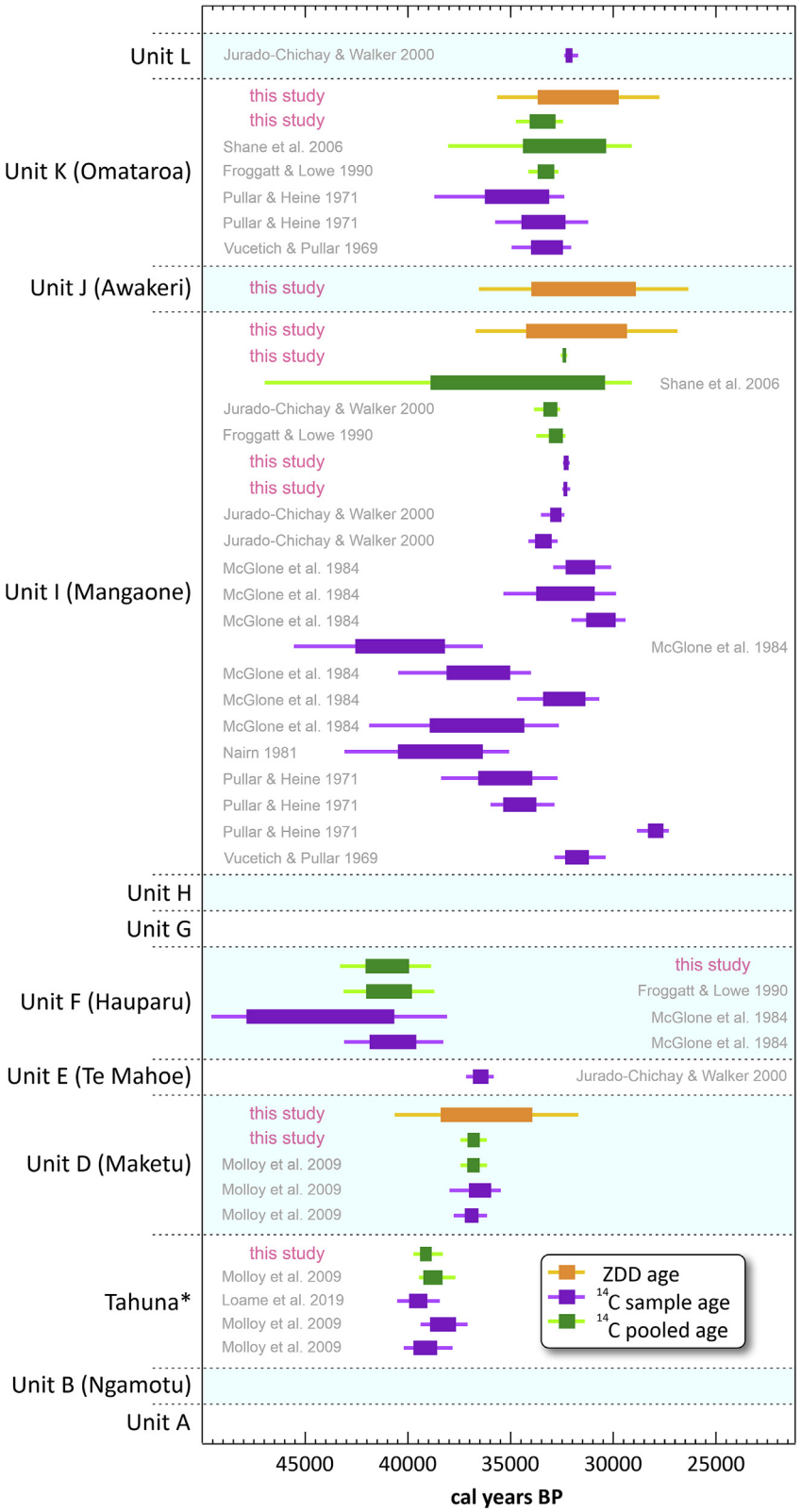

Fig. 3. Summary of published ^{14}C, new ^{14}C, and new ZDD ages for MSg tephras (and Tahuna tephra which did not originate in OVC) arranged in stratigraphic order. The ages are displayed as 1σ (bars) and 2σ (whiskers) age ranges. Conventional ^{14}C ages were calibrated to calendar years (cal years BP) in OxCal 4.3 software (Bronk Ramsey, 2009) using the SHCal13 calibration curve (Hogg et al., 2013). Data compiled from Vucetich and Pullar (1969), Pullar and Heine (1971), Nairn (1981), McGlone et al. (1984), Froggatt and Lowe (1990), Jurado-Chichay and Walker (2000), Shane et al. (2006), Molloy et al. (2009), Loame et al. (2019), and our study.

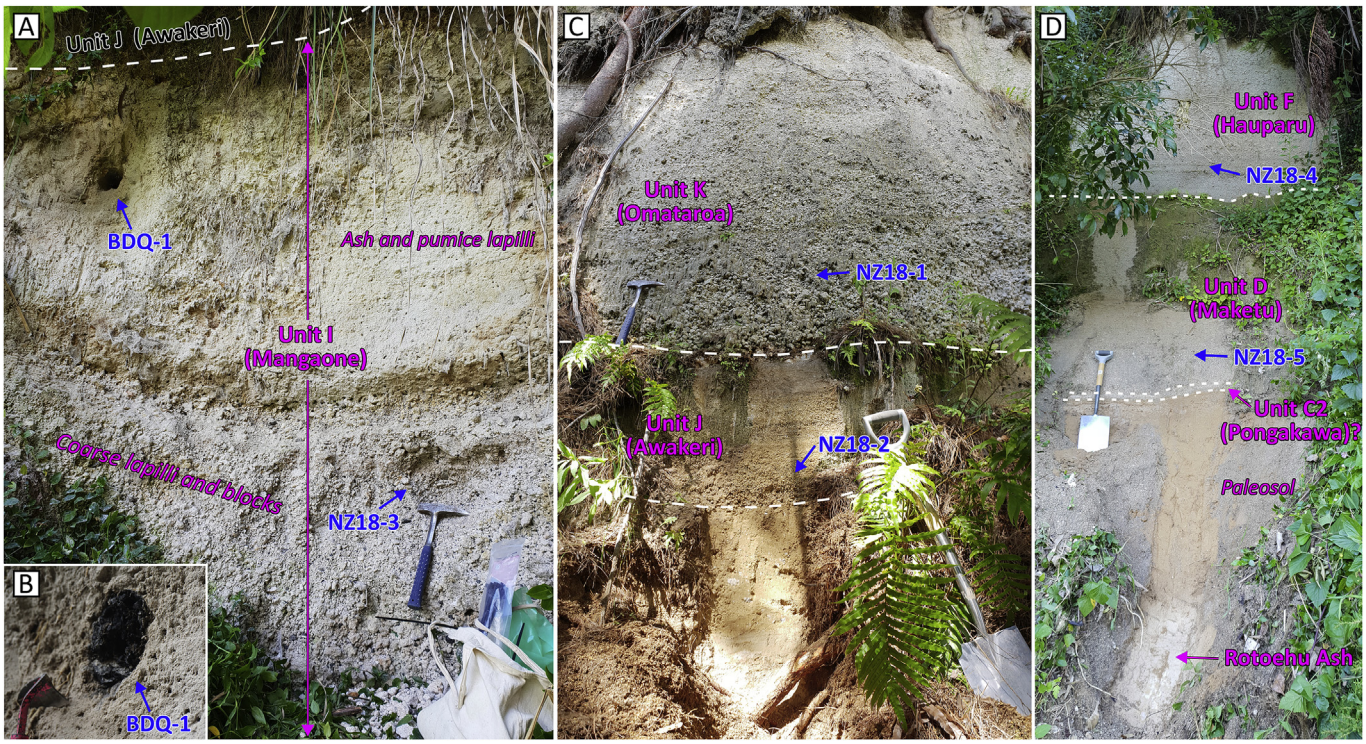

Fig. 4. Images showing the stratigraphy of MSg deposits and the positions of the materials we sampled at two locations for ZDD and ^{14}C dating. A – Unit I (Mangaone) tephra section in Bowditch Quarry was sampled for zircon (NZ18-3) and charcoal (BDQ-1). Uppermost unit (ash and pumice lapilli) was deposited by a pyroclastic flow (density current) (Howorth, 1975). B – Close-up of the BDQ-1 charcoal material. C – Section showing Unit J (Awakeri) and Unit K (Omataroa) tephras in Bowditch Quarry. D – Section at Little Waihi Road sampled for Unit D (Maketu) and Unit F (Hauparu) tephras (the latter did not yield zircon of required quality). Note that Rotoehu Ash represents tephra-fall beds associated with the eruption of the Rotoiti Tephra Formation (Froggatt and Lowe, 1990). Spade for scale is ca. 120 cm long.

based ages from lake sediments and deep-sea cores (Wright et al., 1995; Shane and Sandiford, 2003; Newnham et al., 2004; Shane et al., 2006; Molloy et al., 2009; Nilsson et al., 2011; Peti and Augustinus, 2019).

Another geochronological approach applied to the MSg tephras is optical luminescence dating of paleosols beneath the Tahuna tephra by Lian and Shane (2000), who reported ages of 30 ± 2 and 34 ± 3 ka. These ages, however, are younger than the ^{14}C ages measured on the Tahuna tephra (37.5 ± 0.7 and 38.5 ± 0.6 ka) by Molloy et al. (2009) and therefore are not considered further. Finally, Charlier and Wilson (2010) reported zircon U–Th crystallization ages of $50^{+11}_{-10} - 395^{+\infty}_{-110}$ ka (weighted average: 81 ± 11 ka (95% conf. interval); n = 42; MSWD = 6.4) and $20^{+11}_{-10} - 320^{+250}_{-71}$ ka (weighted average: 51.7 ± 5.9 ka (95% conf. interval); n = 54; MSWD = 3.6) for Unit B (Ngamotu) and Unit I (Mangaone), respectively. The youngest statistically meaningful populations in the age spectra may provide a coarse estimate of the maximum limit for the eruption age of these tephras.

2.4. Stratigraphy of sample sites

Samples of Unit I (Mangaone), Unit J (Awakeri), and Unit K (Omataroa) were collected from the type section for Unit I (Mangaone) tephra in the Bowditch Quarry on State Highway 2 (S38°01′21.6″ E176°43′18.2″), designated by both Howorth (1975, p. 696) and Jurado-Chichay and Walker (2000, p. 326). Here, the exposed sequence consists of (from bottom to top; Fig. 4): paleosol on Unit F (Hauparu); Unit I (Mangaone), a ~5 m thick deposit of massive, weakly-bedded, inversely-graded pumice lapilli and blocks, which is further subdivided into a lower unit (medium-coarse lapilli), middle unit (coarse lapilli and blocks) that we sampled for pumice clasts (sample NZ18-3; Fig. 4A), and an upper pyroclastic flow unit (ash and pumice lapilli) which contains carbonized logs that we sampled for ^{14}C dating (sample BDQ-1; Fig. 4A and B); Unit J (Awakeri) comprising a ~50-cm-thick pumice fall deposit with <1 cm pumice lapilli and dark lithics fining upward. Here we collected a sample (NZ18-2) of coarser pumice from the base of the formation (Fig. 4C); Unit K (Omataroa) comprising a >4 m thick, mostly coarse pumice fall deposit with pumice clasts <5 cm, which we sampled ~20 cm above the lower contact (sample NZ18-1; Fig. 4C); and Kawakawa tephra capping the Mangaone Subgroup sequence.

Samples of Unit F (Hauparu) and Unit D (Maketu) were collected from a reference site exposed on the Little Waihi Road site (S37°45′39.7″ E176°28′20.0″) and described in Briggs et al. (2006, p. 23); type locations for both units are nearby (Jurado-Chichay and Walker, 2000, p. 326). The sequence comprises (from bottom to top; Fig. 4D): Rotoehu Ash (over Rotoiti Ignimbrite); a ~150 cm thick brown paleosol; a distinct, thin (~5 cm thick) white ash layer (possibly Unit C2 (Pongakawa tephra); Briggs et al., 2006); Unit D (Maketu), consisting of a ~1.5 m thick deposit with normally graded, pink-coloured coarse pumice lapilli (our sample NZ18-5; Fig. 4D) and a weak paleosol; Unit F (Hauparu), comprising >2 m thick, coarse plinian-fall deposits containing large pumice clasts up to ~5 cm in diameter (our sample NZ18-4; Fig. 4D).

3. Methods

3.1. ZDD – sample preparation, dating procedure

Prior to zircon separation, ~200 g of pumice clasts from each sample were submitted to Labwest Minerals Analysis Pty Ltd

(Perth) for trace element analysis by solution ICPMS in order to determine the whole rock Th and U abundances required for ZDD age calculation. The samples were pulverized and 100 g of material was microwave digested using a proprietary method in a mixture of HF, HCl, and HNO_3 under high pressure (~20 bar) and temperature (~180 °C) in sealed Teflon pressure vessels. The solutions were analysed for U and Th by external calibration on a Perking Elmer NexION 300Q ICPMS.

The remaining aliquot of the sample was processed for zircon. Zircon was separated from the samples at the John de Laeter Centre (JdLC) at Curtin University following a standard work-flow for heavy mineral separation with some modification: samples were disaggregated to <400 μm fraction using SelFrag disaggregation. This approach requires that samples be submerged in water, so pumice that floated was soaked in water (usually for one week) until it sank. Heavy minerals were pre-concentrated using a Jasper Canyon Research zircon concentrating table. The heavy fractions were dried and processed through heavy liquids using lithium polytungstates (LST; specific gravity = ~2.85 g/cm^3) and magnetic separation. The heavy non-magnetic fraction was then handpicked for zircon under a stereomicroscope. Finally, zircon crystals were rinsed in cold 48% HF for 3 min to remove adherent glass.

Zircon crystals were pressed into indium (In) metal with unpolished crystal faces exposed at the surface. The surface of the mount was levelled and coated with a conductive layer of gold, and crystal rims were dated by U–Th disequilibrium methods with a CAMECA ims 1280-HR (SIMS) at the HIP Laboratory at Heidelberg University, Germany, following the protocols for dynamic multi-collection analysis described in Schmitt et al. (2017) and Friedrichs et al. (2020). ThO^+/UO^+ relative sensitivities were calibrated on 91500 (Wiedenbeck et al., 1995) and AS3 (Paces and Miller, 1993) zircon crystals, used as primary and secondary calibration standards, respectively. The weighted average of $^{230}Th/^{238}U$ values obtained on AS3 analyses bracketing blocks of the unknowns is 1.005 ± 0.005 (1σ; MSWD = 0.93; n = 49), consistent with secular equilibrium of AS3. The dimension of elliptical craters sputtered on the crystal rims with a ~40 μm wide ion beam were ~40 (length) × 25 (width) × 4 μm (depth), preserving >98% of the crystal volume for subsequent (U–Th)/He analysis (Fig. 1). Zircon U–Th model ages were calculated as two-point isochrons regressed through measured $^{238}U/^{230}Th$ values and whole rock Th/U composition that was assumed as representative for the melt composition.

After the SIMS analysis, mounts were wiped with methanol to remove the gold coating, and zircon crystals were plucked out of the In ahead of (U–Th)/He dating in the JdLC Low-Temperature Thermochronology Facility (Curtin University) following the procedures described in Danišík et al. (2012, 2017a). The crystals were photographed, measured for physical dimensions, transferred and packed into niobium (Nb) microtubes and loaded into an Alphachron II instrument for He extraction. ^4He together with other gases were extracted at ~1250 °C under ultra-high vacuum using a diode laser, cleaned on Ti–Zr getters, and spiked with 99.9% pure ^3He gas. The volume of ^4He was measured by isotope dilution on a QMG 220 M1 Pfeiffer Prisma Plus mass spectrometer. A "re-extract" was run after each analysis to verify complete outgassing of the crystal. Helium gas signals were corrected for blank, determined by analysing empty Nb microtubes interspersed between the unknowns using the same gas extraction procedure. After the He measurements, Nb microtubes containing the crystals were retrieved from the Alphachron, spiked with ^{235}U and ^{230}Th, and dissolved in Parr acid digestions vessels in two cycles of HF, HNO_3 (cycle 1), and HCl acids (cycle 2) following the procedures described in Evans et al. (2005). Sample, blank, and spiked standard solutions were then diluted with Milli-Q water and analysed by isotope dilution for ^{238}U and ^{232}Th, and by external calibration for ^{147}Sm on an Element XR™ High Resolution ICP-MS. The total analytical uncertainty (TAU) was calculated as a square root of sum of squares of uncertainty on He and weighted uncertainties on U, Th, and Sm measurements. The zircon (U–Th)/He ages were corrected for alpha ejection (F_t-correction) after Farley et al. (1996), whereby homogenous distributions of U, Th, and Sm were assumed for the crystals. The accuracy of the zircon (U–Th)/He dating procedure was monitored by replicate analyses of internal standard Fish Canyon Tuff zircon where crystals measured over the course of this study yielded a mean (U–Th)/He age of 28.5 ± 0.3 Ma (1σ; MSWD = 1.03; n = 13), in excellent agreement with the reference (U–Th)/He age of 28.3 ± 1.3 Ma (Reiners, 2005).

The F_t-corrected (U–Th)/He ages were then corrected for U-series disequilibrium and pre-eruptive crystal residence time (Farley et al., 2002) using MCHeCalc software (Schmitt et al., 2010b). In addition to the F_t-corrected (U–Th)/He ages and U–Th crystallization ages (with their associated uncertainties), the software also requires D_{230} and D_{231} parameters which describe zircon-melt fractionation of Th and Pa relative to U. Calculation of D_{230} (Farley et al., 2002) was made by dividing zircon Th/U values by whole-rock Th/U, whereby we assume that the magma was in secular equilibrium and that the measured whole-rock values are representative for the magma from which the zircons originated. For D_{231} a value of 3.3 was adopted based on an average of published Pa/U zircon-rhyolite melt partition coefficient values (Schmitt, 2007, 2011; Sakata et al., 2017). Disequilibrium-corrected (U–Th)/He ages (7–9 replicates per sample) were then used to calculate a mean value, which is interpreted as the representative eruption age of each sample (and termed ZDD eruption age). This was done by applying two different approaches. In the first, traditionally used 'frequentist approach', the error-weighted means with 95% confidence intervals were calculated using Isoplot v.4.15 Excel add-in (Ludwig, 2012). In the second (novel) 'Bayesian approach', we applied a Bayesian probability model to predict

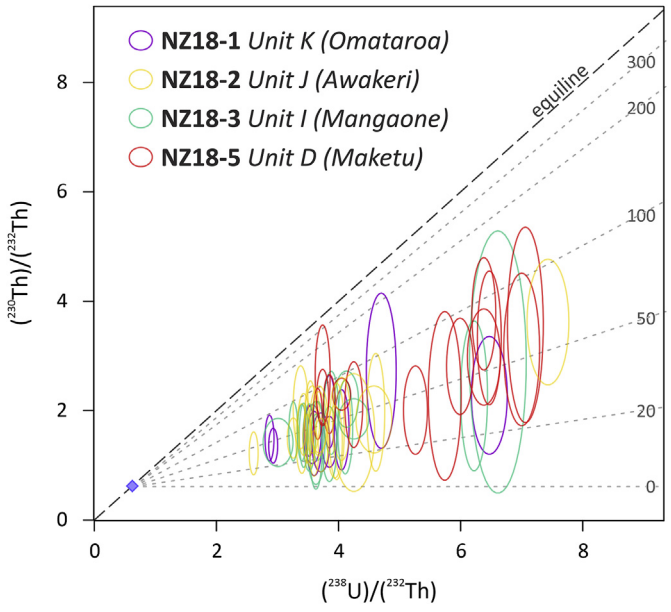

Fig. 5. ^{238}U–^{230}Th isochron diagram for MSg tephras dated in this study showing that all zircon isotopic ratios are in secular disequilibrium (i.e., all ellipses plot to the right of the equiline). Confidence ellipses are plotted at 95% level of confidence. The diagram was constructed in IsoplotR (Vermeesch, 2018); isochrons (dashed grey lines) are based on mean Th/U whole rock composition of 0.639 (blue diamond). (For interpretation of the references to colour in this figure legend, the reader is referred to the Web version of this article.)

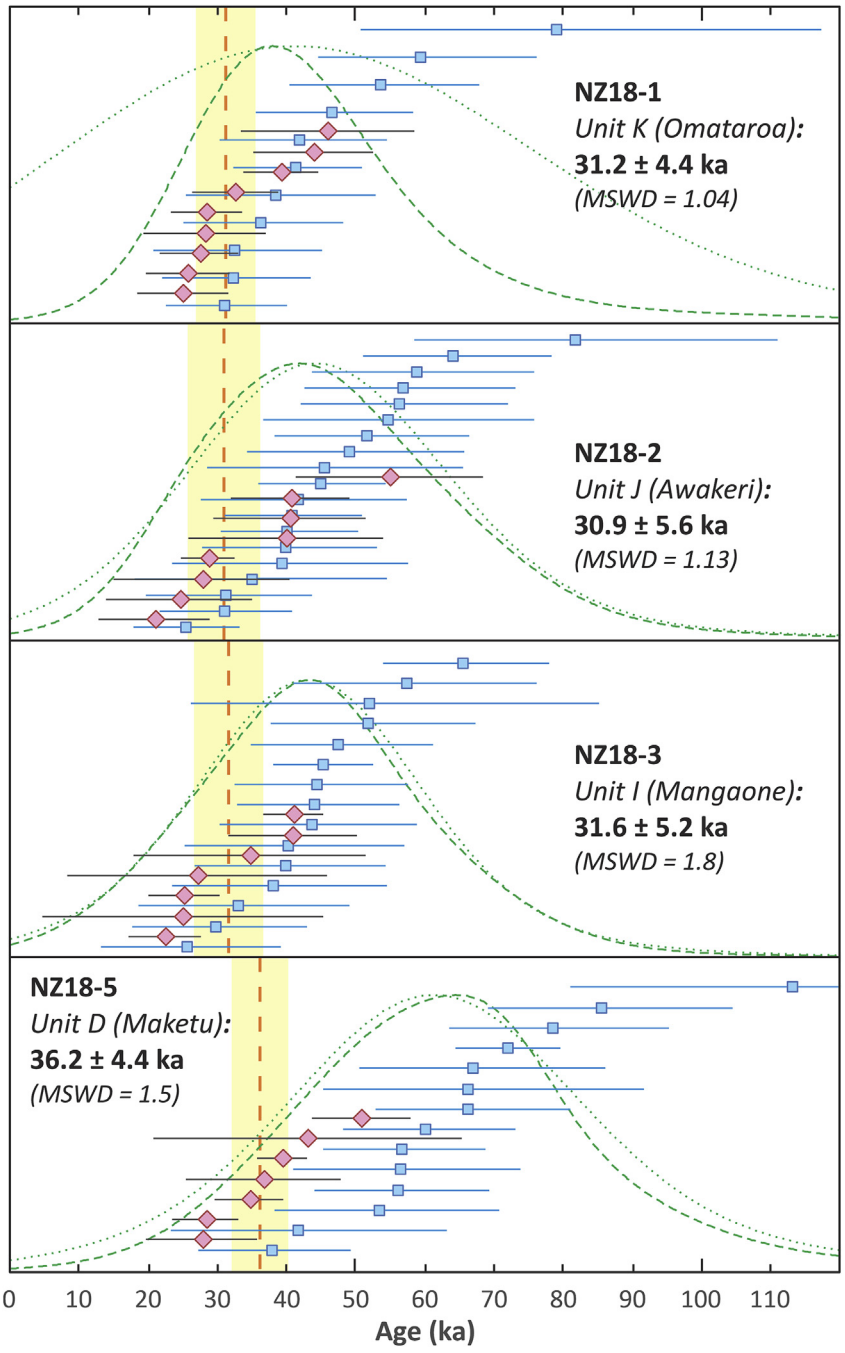

Fig. 6. Zircon U–Th and (U–Th)/He ages (blue squares and red diamonds, respectively) with 1σ analytical uncertainties for MSg tephras analysed by ZDD displayed in ranked order plots. Kernel density estimation (KDE) and probability distribution function (PDF) curves (dotted and dashed green curves, respectively) for U–Th data were constructed in DensityPlotter (Vermeesch, 2012). Vertical dashed orange lines and yellow rectangles indicate the ZDD eruption ages and their 95% confidence intervals, respectively, calculated as error weighted means in Isoplot (Ludwig, 2012). The samples are arranged in stratigraphic order to allow easy comparison of the ZDD eruption ages. MSWD – mean square of weighted deviation. The full dataset can be found in Table 3 and Supplementary Tables S2 and S3. (For interpretation of the references to colour in this figure legend, the reader is referred to the Web version of this article.)

posterior mean values and their 95% high density intervals (HDI). In addition, we also applied Bayesian analysis for comparing two groups, which is similar to the Bayesian *t*-test of Kruschke (2013), but was modified so that it takes into account uncertainties of the measured data following the approach of Gelman et al. (2013) applied to the "eight schools" example, to test whether there is a statistically significant difference between the ZDD ages obtained on different tephras.

To enable direct comparison of ZDD eruption ages with ^{14}C ages, conventional ZDD eruption ages were converted to calendar kilo-years before present (ka BP), where present = 1950 CE.

3.2. ^{14}C dating procedure

Two aliquots of charcoal sample BDQ-1 from Unit I (Mangaone) tephra were analysed by liquid scintillation spectroscopy at the

Table 3
ZDD data summary.

Sample code	^{232}Th (ng)	± (%)	^{238}U (ng)	± (%)	^{147}Sm (ng)	± (%)	^{4}He (ncc)	± (%)	TAU (%)	Th/U	Raw He age (ka)	±1σ (ka)	F_t	± (%)	F_t-cor. He age (ka)	±1σ (ka)	U–Th (ka)	±1σ (ka)	D_{230}	Diseq.-cor. He age (ka BP)	±1σ (ka)
Unit K (Omataroa)																					
NZ18-1-1	0.308	2.0	0.402	2.4	0.00052	1.1	0.0007	19.7	19.8	0.76	12.7	2.5	0.78	5	16.3	3.3	36.0	12.2	0.1604	27.2	5.7
NZ18-1-2	0.164	1.4	0.190	2.3	0.00023	1.5	0.0007	15.2	15.3	0.86	25.4	3.9	0.76	5	33.3	5.4	78.9	38.3	0.1806	43.8	8.6
NZ18-1-3	0.367	1.3	0.368	1.9	0.00066	0.9	0.0007	21.5	21.6	0.99	12.9	2.8	0.73	5	17.8	3.9	59.2	17.0	0.2087	25.5	6.1
NZ18-1-7	0.386	1.3	0.347	2.0	0.00071	0.8	0.0008	18.0	18.1	1.11	14.2	2.6	0.66	5	21.5	4.0	41.6	12.8	0.2330	32.4	6.2
NZ18-1-8	0.366	2.1	0.395	2.5	0.00082	1.1	0.0008	16.2	16.3	0.92	13.0	2.1	0.71	5	18.4	3.1	46.3	11.9	0.1938	28.3	5.2
NZ18-1-9	0.285	1.4	0.239	2.1	0.00112	1.2	0.0004	30.0	30.0	1.18	11.8	3.5	0.63	5	18.6	5.7	41.1	9.7	0.2494	28.1	8.9
NZ18-1-10	0.187	1.4	0.192	1.9	0.00068	0.9	0.0006	28.9	29.0	0.96	21.3	6.2	0.72	5	29.7	8.7	38.3	14.6	0.2033	45.8	12.6
NZ18-1-12	0.253	1.4	0.247	2.0	0.00032	1.2	0.0004	25.7	25.7	1.02	11.1	2.9	0.71	5	15.7	4.1	32.1	11.3	0.2141	24.8	6.6
NZ18-1-13	0.315	2.0	0.378	2.5	0.00054	1.3	0.0010	13.7	13.9	0.83	18.2	2.5	0.77	5	23.6	3.5	30.9	9.1	0.1741	39.0	5.4
															Weighted mean (in ka BP) ± 95% conf. (in ka) *(MSWD)*:					**31.2 ± 4.4** *(1.04)*	
															Posterior mean (in ka BP) ± 95% HDI (in ka):					**31.1 + 4.3/-4.2**	
Unit J (Awakeri)																					
NZ18-2-18	0.181	1.4	0.190	2.0	0.00035	1.3	0.0004	44.3	44.3	0.94	14.6	6.5	0.72	5	20.1	9.0	81.6	29.4	0.1886	27.7	12.7
NZ18-2-10	0.225	1.4	0.192	2.1	0.00043	1.3	0.0003	42.2	42.3	1.16	10.8	4.6	0.69	5	15.7	6.7	25.2	7.9	0.2317	24.4	10.5
NZ18-2-11	0.108	1.4	0.142	2.0	0.00008	1.7	0.0004	25.8	25.9	0.75	20.1	5.2	0.60	5	33.5	8.8	40.5	10.4	0.1505	54.7	13.5
NZ18-2-12	0.269	2.2	0.376	2.6	0.00032	2.9	0.0005	36.8	36.9	0.71	9.5	3.5	0.75	5	12.8	4.8	34.8	19.7	0.1416	20.8	8.1
NZ18-2-16	0.527	1.3	0.502	2.1	0.00127	1.2	0.0011	10.8	10.9	1.04	14.6	1.6	0.78	5	18.8	2.3	41.5	15.9	0.2082	28.5	3.9
NZ18-2-8	0.293	1.4	0.290	2.0	0.00028	1.7	0.0008	19.6	19.7	1.00	19.3	3.8	0.71	5	27.1	5.5	51.4	14.9	0.2002	40.4	8.5
NZ18-2-7	0.162	1.4	0.129	2.0	0.00006	2.5	0.0003	27.8	27.8	1.24	16.3	4.5	0.61	5	26.9	7.6	39.7	13.4	0.2486	40.3	11.0
NZ18-2-13	0.152	1.9	0.153	2.4	0.00035	1.6	0.0004	41.1	41.2	0.99	16.2	6.7	0.65	5	24.7	10.3	30.8	10.0	0.1970	39.8	14.1
															Weighted mean (in ka BP) ± 95% conf. (in ka) *(MSWD)*:					**30.9 ± 5.6** *(1.13)*	
															Posterior mean (in ka BP) ± 95% HDI (in ka):					**30.8 + 5.5/-5.4**	
Unit I (Mangaone)																					
NZ18-3-18	0.124	1.4	0.105	2.1	0.00022	1.3	0.0003	47.5	47.6	1.17	16.7	7.9	0.65	5	25.7	12.3	81.6	29.4	0.2439	34.5	16.7
NZ18-3-1	0.092	1.5	0.089	2.3	0.00018	2.5	0.0002	62.0	62.1	1.03	11.6	7.2	0.61	5	19.0	11.8	43.9	12.4	0.2136	27.0	18.7
NZ18-3-7	0.092	1.5	0.084	2.1	0.00014	1.9	0.0002	71.7	71.7	1.09	12.3	8.8	0.65	5	18.8	13.5	51.5	15.7	0.2278	24.9	20.3
NZ18-3-8	0.329	1.9	0.275	2.4	0.00086	0.9	0.0004	22.4	22.5	1.19	9.3	2.1	0.63	5	14.7	3.4	29.5	13.4	0.2474	22.2	5.2
NZ18-3-14	0.532	1.3	0.727	2.0	0.00080	1.3	0.0019	7.7	7.9	0.73	18.2	1.4	0.72	5	25.3	2.4	47.2	13.9	0.1512	40.9	4.3
NZ18-3-16	0.250	1.4	0.256	2.2	0.00081	0.9	0.0006	18.2	18.2	0.97	16.3	3.0	0.59	10	27.7	5.8	65.3	12.6	0.2021	40.7	9.3
NZ18-3-13	0.298	1.4	0.391	2.0	0.00051	1.3	0.0006	17.7	17.8	0.76	11.1	2.0	0.72	5	15.5	2.9	39.6	14.6	0.1575	25.0	5.1
															Weighted mean (in ka BP) ± 95% conf. (in ka) *(MSWD)*:					**31.5 ± 5.2** *(1.8)*	
															Posterior mean (in ka BP) ± 95% HDI (in ka):					**31.5 + 5.1/-5.1**	
Unit D (Maketu)																					
NZ18-5-3	1.638	2.1	1.212	2.5	0.00087	1.0	0.0047	5.4	5.7	1.34	24.2	1.4	0.81	5	30.1	2.3	78.2	17.0	0.2994	39.3	3.6
NZ18-5-4	0.586	1.3	0.730	2.0	0.00084	1.3	0.0016	13.7	13.8	0.80	15.2	2.1	0.76	5	19.8	2.9	66.0	14.9	0.1777	28.2	4.8
NZ18-5-11	0.100	1.5	0.146	2.0	0.00004	2.7	0.0004	28.2	28.3	0.68	17.6	5.0	0.72	5	24.5	7.0	66.8	19.2	0.1507	36.5	11.3
NZ18-5-10	0.402	1.9	0.411	2.4	0.00023	1.2	0.0010	11.7	11.9	0.97	16.8	2.0	0.71	5	23.6	3.0	56.4	12.3	0.2165	34.5	4.9
NZ18-5-9	0.192	1.4	0.204	2.0	0.00016	2.2	0.0004	27.2	27.2	0.93	13.5	3.7	0.72	5	18.7	5.2	41.4	21.8	0.2085	27.6	8.0
NZ18-5-15	0.418	1.9	0.316	2.4	0.00005	1.7	0.0012	12.8	13.0	1.31	23.5	3.1	0.64	5	36.6	5.1	53.2	17.5	0.2930	50.6	7.1
NZ18-5-12	0.076	1.5	0.082	2.0	0.00016	2.2	0.0002	47.8	47.8	0.92	16.1	7.7	0.55	10	29.5	14.4	55.9	13.3	0.2048	42.9	22.3
*NZ18-5-17**	0.085	1.5	0.086	2.0	0.00006	2.6	0.0001	160.8	160.8	0.98	7.2	11.6	0.49	15	14.7	23.8					
															Weighted mean (in ka BP) ± 95% conf. (in ka) *(MSWD)*:					**36.1 ± 4.4** *(1.5)*	
															Posterior mean (in ka BP) ± 95% HDI (in ka):					**36.1 + 4.3/-4.3**	

TAU - total analytical uncertainty; F_t - alpha ejection correction factor calculated after Farley et al. (1996) for homogeneous distribution of parent nuclides; uncertainty on F_t factors was arbitrarily set to 5% and 10% for crystals with $F_t \geq 0.6$ and $F_t < 0.6$, respectively, after Ehlers and Farley (2003), and propagated in quadrature into final age uncertainty; D_{230} - Th zircon-melt fractionation factor calculated after (Farley et al., 2002) using the Th/U ratios of analysed bulk zircon crystals and whole rock Th/U (NZ18-1 = 4.7459; NZ18-2 = 5.057; NZ18-3 = 4.8033; NZ18-5 = 4.4819); Diseq.-cor. (U–Th)/He age (ka BP) - disequilibrium-corrected (U–Th)/He age calculated by MCHeCalc program (Schmitt et al., 2010b) assuming $D_{231} = 3.3$ (i.e., an average of $f_{Pa/U}$ values published by Schmitt, 2007, 2011; Sakata et al., 2017) and converted to calendar kiloyears before present (ka BP), where present = 1950 CE; Eruption ages were calculated (i) as error weighted average by Isoplot v.4.15 Excel add-in (Ludwig, 2012) and (ii) posterior mean value predicted Bayesian probability model. Crystal marked with asterisk was disregarded because of its high analytical uncertainty.

Waikato Radiocarbon Dating Laboratory (New Zealand) following the methods described in Hogg et al. (2007). The analysis utilized acid–base–acid pre-treatment. The $\delta^{13}C$ values were measured as −21.2 ± 0.2‰. Background blank correction (equivalent to an apparent age of 54.1 ka BP) was achieved by ^{14}C analysis of MIS 5 (~120 ka) wood (Hogg et al., 2007). The resulting conventional ^{14}C age (^{14}C yr BP) was calibrated to calendar years (cal yr BP) by OxCal 4.3 (Bronk Ramsey, 2009) using the SHCal13 calibration curves (Hogg et al., 2013). Previously published ^{14}C ages were calibrated to calendar years by the same procedure to enable comparison with our new ZDD and ^{14}C results.

3.3. Age sequence modelling using Bayesian inference

To reconstruct a robust eruptive chronology for the MSg sequence in its entirety, a Bayesian 'target event date model' (Lanos and Philippe, 2017, 2018) incorporating ZDD and ^{14}C geochronological data, as well as stratigraphic information, was developed in ChronoModel v. 2.0 software (Lanos and Dufresne, 2019). This software was originally designed for archaeological purposes to estimate the date of events by combining numerical (absolute) dates obtained (often by different methods) on archaeological artefacts, as well as relative dates inferred from their stratigraphic positions. These data can be used as prior information for the modelling, which is based on a hierarchical Bayesian statistical approach and utilizes Markov chain Monte Carlo (MCMC) numerical techniques to estimate the dates of target events and their uncertainties. One of the major advantages of the target event date model (Lanos and Philippe, 2017, 2018) over other Bayesian chronological modelling packages such as OxCal and BCal is in the

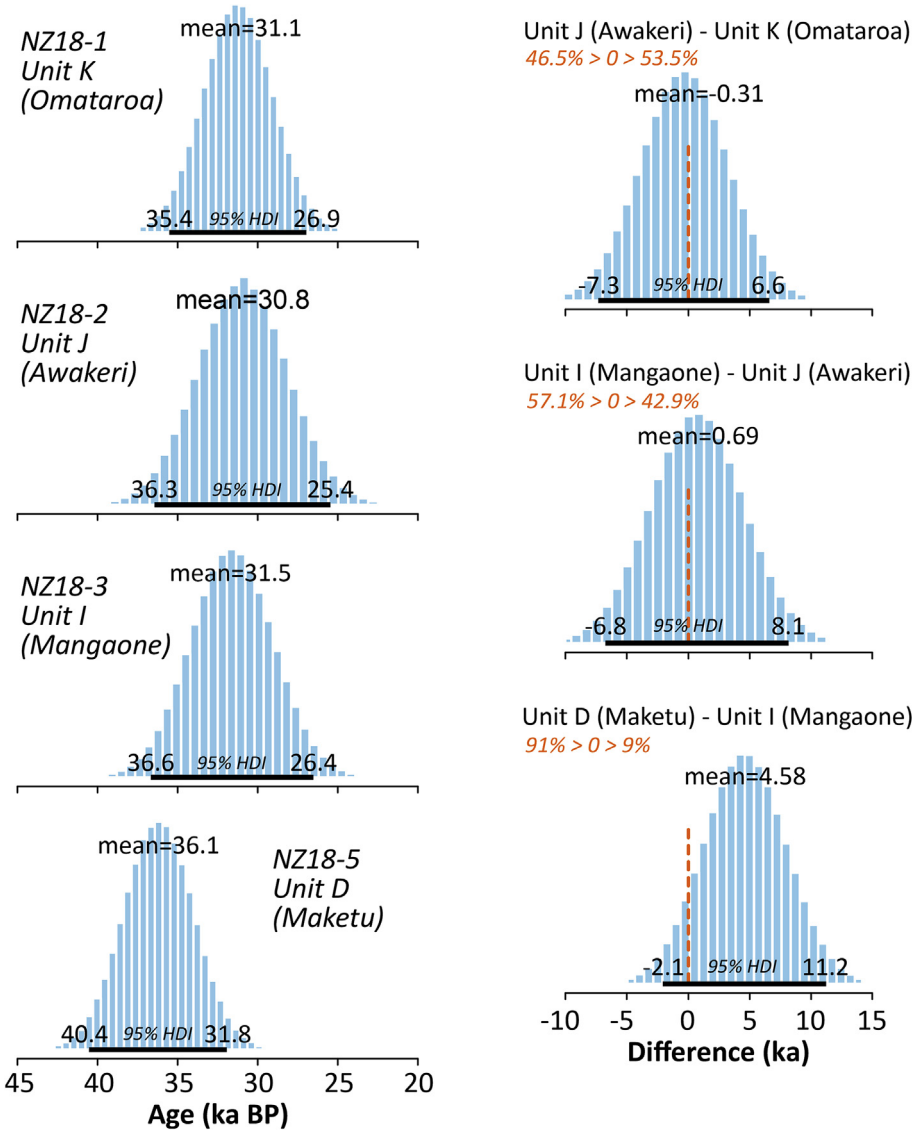

Fig. 7. *Left*: Histograms showing posterior distributions of mean values for (U–Th)/He ages that represent the Bayesian estimates of most probable eruption ages and their uncertainties (horizontal bars represent 95% high density intervals, HDI). *Right*: Histograms showing posterior differences of the mean (U–Th)/He values predicted by Bayesian analysis for stratigraphically adjacent tephras. The differences of the mean values serve as a test to decide whether there is a credible difference between the eruption ages of the dated tephras. For Units I (Mangaone), J (Awakeri), and K (Omataroa), the 95% HDI of the difference of means are quasi-symmetrically distributed around zero, and there is no statistically credible difference in their eruption ages. For Units D (Maketu) and I (Mangaone) (bottom right diagram), in contrast, the 95% HDI marginally overlaps with zero and >90% of the predicted values are >0, and therefore we can conclude that there is >90% probability that the eruption ages of these two tephras are credibly different.

robustness of predicted dates that yield a less precise but more accurate reflection of the chronology (Lanos and Philippe, 2018).

The schematic structure of the MSg tephra model can be found in Supplementary Figure S1, and input data are listed in Supplementary Table S1. In the model, tephras were defined as separate events characterized by ZDD and/or ^{14}C data (i.e., ages and 1σ uncertainties) from this study or published literature. Tephras with no available radiometric data were loosely constrained as uninformative dates, ranging from the oldest age of the underlying unit to youngest age of the overlying unit. The relative chronology of the events was constrained based on stratigraphic superpositioning. Maximum and minimum age limits of the whole sequence were constrained by the eruption ages of the Rotoiti Tephra and Earthquake Flat Tephra formations (45.2 ± 1.65 and 45.2 ± 1.45 ka (1σ), respectively; Danišík et al., 2012) and Oruanui/Kawakawa tephra (25.4 ± 0.1 cal ka BP; Vandergoes et al., 2013), bracketing the MSg sequence. We ran three MCMC sampling chains consisting of 1000 burn-in, 10,000 adaptation, and 100,000 acquisition iterations; thinning rate was set to 10. The model calculates posterior distributions for event dates that are described by a range of parameters; for simplicity we will refer to mode of the posterior distribution (MAP or maximum *a posterior* probability) and 95% highest posterior density (HPD) region estimates (i.e., an analogue to 2σ uncertainty range in frequentist statistics) as representative values for the posterior event dates.

4. Results

4.1. U–Th crystallization ages

In total, four samples were dated by ZDD; one sample NZ18-4 (Unit F, Hauparu) yielded only a few small zircon crystals (<40 μm in diameter) of inadequate size for ZDD. Analytical results are summarized in Supplementary Table S2. Analyses of all crystal surfaces revealed ^{230}Th deficits; (^{230}Th)/(^{238}U) values (parentheses indicate activities) are below unity, with data plotting to the right of the equiline (Fig. 5), suggesting a crystallization age ≪350 ka for all 59 dated crystals. U–Th model ages defined by zircon and whole rock compositions range from ca. 25 ± 8 to 113 ± 39 ka (1σ). U–Th age spectra (Fig. 6) for all four samples are unimodal with mean values of ca. 40 ka for the stratigraphically higher samples (Unit I (Mangaone), Unit J (Awakeri), Unit K (Omataroa)) and ca. 60 ka for the stratigraphically lowest (oldest) sample, Unit D (Maketu).

4.2. (U–Th)/He ages

Seven to nine SIMS-dated zircon crystals per sample were dated by the (U–Th)/He method. Alpha-ejection corrected (U–Th)/He ages are younger than their corresponding U–Th ages for all 33 double-dated crystals (Table 3; Supplementary Table S3). One crystal (NZ18-5-17) had an extremely large analytical uncertainty (160%; 1σ) due to the low He content and was rejected from further evaluation. The remaining F_t-corrected (U–Th)/He ages, corrected for disequilibrium, yield weighted mean ages (arranged in stratigraphical order from bottom to top) as follows: Unit D (Maketu) 36.1 ± 4.4 ka BP (95% conf.; MSWD = 1.5; n = 7); Unit I (Mangaone) 31.5 ± 5.2 ka BP (MSWD = 1.8; n = 7); , Unit J (Awakeri) 30.9 ± 5.6 ka BP (MSWD = 1.13; n = 8); and Unit K (Omataroa) 31.2 ± 4.4 ka BP (MSWD = 1.04; n = 9) (Fig. 6; Table 3). The weighted mean ages and their uncertainties are almost identical to the posterior mean values and 95% HDIs determined by Bayesian inference (Fig. 7; Table 3). Individual grain ages are reproducible within analytical uncertainty (Figs. 6 and 7) and the MSWD values (~1–1.8) are in the acceptable range of a reduced chi-squared test for sample sizes of 7–9 (Spencer et al., 2016). Therefore, the data for each sample are interpreted to represent a single population and the weighted mean values are our best estimates of ZDD eruption ages.

Due to the large age uncertainties, the relationship between the ZDD ages and relative stratigraphic position of the tephras that were sampled is not very clear. Bayesian inference revealed that only the sample from Unit D (Maketu), with the lowest position in the stratigraphic sequence and the oldest ZDD age, is statistically different from the upper three tephras, which yielded statistically indistinguishable ZDD ages (Fig. 7). The statistical overlap in ages is not surprising given that paleosols formed on each unit are thin and weakly developed (Jurado-Chichay and Walker, 2000). The weak paleosols represent periods of volcanic quiescence (paraconformities mark the boundary between the buried paleosol top and overlying tephra) that likely correspond to a few decades to centuries (Jurado-Chichay and Walker, 2000), through to a maximum of a few thousand years based on clay contents and thicknesses (Hodder et al., 1990; Lowe and Percival, 1993; Lowe and Hogg, 1995).

4.3. ^{14}C ages

Two aliquots of sample BDQ-1 (Unit I (Mangaone)) yielded conventional ^{14}C ages of 26,846 ± 117 and 26,892 ± 117 yr BP (1σ), calibrated to 2σ probability age ranges of 30,752–31,150 and 30,777–31,171 cal yr BP, respectively (Table 2; Supplementary Table S4). These ages are in good agreement with high-precision ^{14}C 2σ age ranges of 31,095–32,357 and 31,456–33,003 cal yr BP on charcoal reported for the same tephra by Jurado-Chichay and Walker (2000) (Table 2). Therefore, we combined these four ages using the R_combine function in OxCal 4.3 and calculated a pooled 2σ age range of 30,902–31,247 cal yr BP (2σ age range), which is considered our optimum ^{14}C eruption age estimate for Unit I (Mangaone). We did not include other published ^{14}C ages because of their lower precision or problems with sample material as discussed in Froggatt and Lowe (1990) and Jurado-Chichay and Walker (2000).

5. Interpretation and discussion

5.1. Comparison of ZDD eruption ages and ^{14}C ages

The new ZDD eruption ages are in excellent agreement with the corresponding ^{14}C ages. Both methods yielded statistically indistinguishable ages, fully overlapping within 2σ uncertainty. For Unit D (Maketu), the ZDD age of 36.1 ± 4.4 ka BP overlaps with the ^{14}C 2σ age range of 35.2–36.6 cal ka BP (Molloy et al., 2009). For Unit I (Mangaone), the ZDD age of 31.5 ± 5.2 ka BP is concordant with the preferred optimum ^{14}C 2σ age range of 30.9–31.2 cal ka BP based on pooled high-precision ^{14}C data obtained on charcoal from Jurado-Chichay (2000) and our study. The ZDD age of 30.9 ± 5.6 ka BP is the first radiometric age reported for Unit J (Awakeri), and is concordant with the bracketing ^{14}C 2σ age ranges of 30.9–31.2 and 31.2–33.7 cal ka BP from underlying Unit I (Managone) and

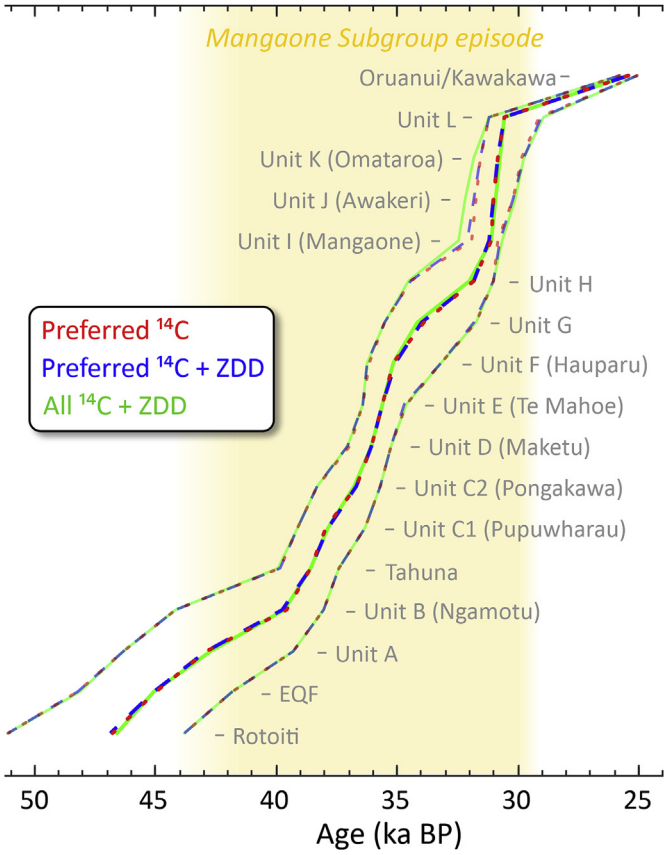

Fig. 8. Comparison of Bayesian age sequence modelling results based on different input parameters as specified in the text. Note the insignificant difference in ages (solid lines) and 95% HPD regions between the three tested models (see text), demonstrating the robustness of the adopted Bayesian approach and its immunity to anomalous ages. Numerical results can be found in Supplementary Table S4.

overlying Unit K (Omataroa), respectively. The 31.2–33.7 cal ka BP 2σ age range for Unit K (Omataroa) overlaps with the ZDD age of 31.2 ± 4.4 ka. The concordance of ages from two independent radiometric dating methods suggests that both methods are accurate because they are dating the same eruption event (as determined by stratigraphy). Accepting the optimum ^{14}C ages as the 'gold standard' for eruption age estimation, the excellent agreement of ^{14}C ages and ZDD ages demonstrates the accuracy of eruption ages derived by ZDD.

The precision of the ZDD eruption ages (i.e., 12–18% age uncertainties at 2σ) is lower than typical ZDD uncertainties of 5–12% (2σ) reported in literature. The precision of ZDD eruption ages is usually related to (over-)dispersion of single crystal (U–Th)/He ages associated with complexities inherent in (U–Th)/He dating systematics (Vermeesch, 2010; Danišík et al., 2017b), and not to the analytical uncertainty of actual measurements. In the case of the data for the MSg tephra sequence generated in this work, the dispersion of single crystal (U–Th)/He ages is not large, with MSWD values close to unity. Instead, the major source of ZDD uncertainty stems from the low He content (and hence large uncertainty associated with He measurements; Table 3), which is related to the young cooling age of the crystals, and to an unusually low U content (ca. 100 ppm on average), significantly lower than typical U concentrations in zircon (300–600 ppm; e.g., Wagner and Van den haute, 1992).

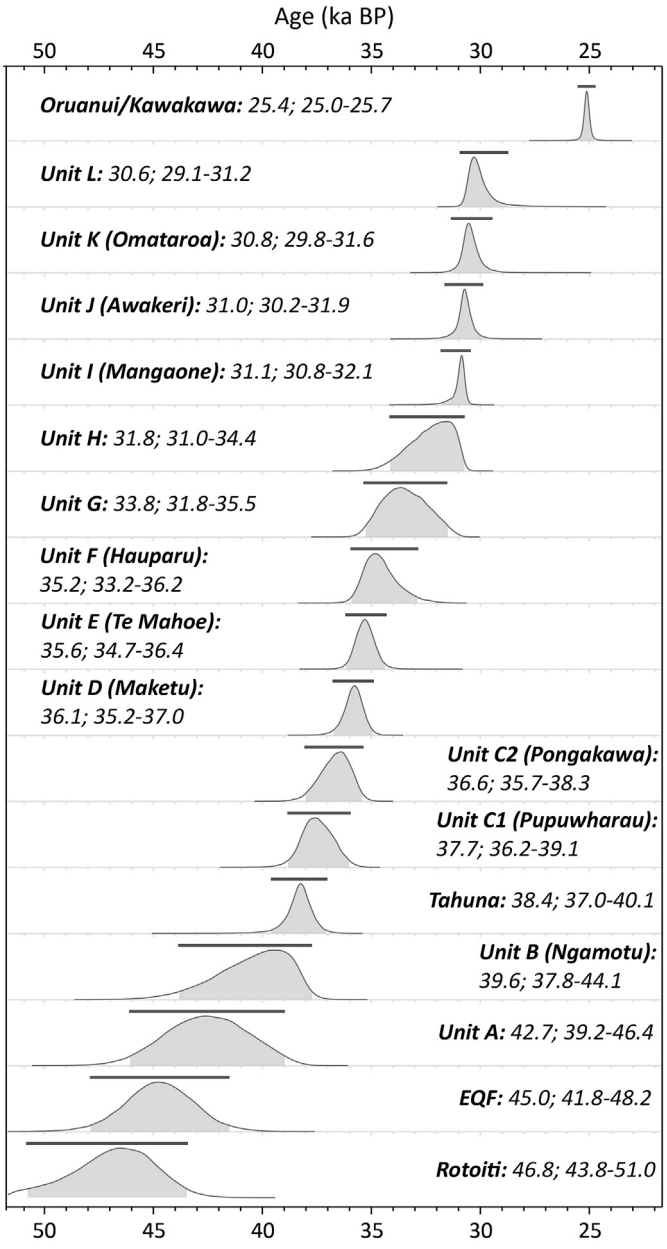

Fig. 9. Posterior distribution graphs for probability densities (curves) of the eruption ages predicted by Bayesian age sequence model in ChronoModel v. 2.0. The 95% highest posterior density (HDP) regions are represented by the horizontal bars above the curves and by the grey filled areas under the curves. *Labels*: name of the eruption/tephra; the mode of the posterior distribution (i.e., maximum a posterior probability or 'MAP') in cal ka BP; 95% HPD in cal ka BP. Numerical results can be found in Supplementary Table S4.

Although the ZDD ages are accurate, precision could likely have been improved by increasing the number of dated crystals. In this study we aimed for 7 to 9 crystals to be double-dated per sample. While we acknowledge that some studies dated up to ~20 replicates per sample in order to achieve high precision ZDD eruption ages (e.g., Danišík et al., 2012; Coble et al., 2017), we nevertheless considered 7–9 crystals an adequate number to obtain the desired precision of 5–12% (2σ) following the example of some other studies (e.g., Schmitt et al., 2011; Molnár et al., 2018). To test whether a larger number of grains per sample would improve precision, we combined the disequilibrium corrected (U–Th)/He ages of samples NZ18-1, NZ18-2, and NZ18-3, respectively, from Unit I (Mangaone), J (Awakeri), K (Omataroa), i.e., samples with overlapping eruption ages. The resulting weighted mean values of 31.0 ± 3.4 ka (NZ18-1 and NZ18-2 combined; n = 17; MSWD = 1.01) and 31.2 ± 2.9 ka (all 3 samples combined; n = 24; MSWD = 1.17) have an uncertainty of 11% and 9.2%, respectively, which are within our desired precision range for the ZDD approach. These results also show that analysing ~15 crystals of low-U MSg zircon per sample should suffice to generate reasonably precise ages.

The new data demonstrate the capability of ZDD to yield accurate eruption ages. Nevertheless, it should be noted that ZDD accuracy can be affected by several factors. These include the presence of mineral or fluid inclusions potentially leading to older than expected (U–Th)/He ages (e.g., Danišík et al., 2017b), incomplete resetting of xenocrysts (e.g., Blondes et al., 2007; Ulusoy et al., 2019), heterogeneous distribution of parent nuclides impacting the alpha ejection correction (Hourigan et al., 2005; Danišík et al., 2017b), and simplified assumptions about duration of zircon crystallization and parental melt composition potentially affecting the magnitude of disequilibrium correction (Schmitt, 2011; Storm et al., 2012; Boehnke et al., 2013; Danišík et al., 2017a). In our study, we followed a routine, well-established workflow and used optical microscopy to select euhedral, inclusion free crystals. However, no special effort was made to characterize crystal interiors for U–Th zonation or complexity of crystallization history. Although this "rudimentary" approach arguably yielded accurate ZDD eruption ages as demonstrated by the concordance with ^{14}C data, we emphasize that more detailed crystal characterization may be critical in other ZDD studies.

5.2. Eruption age sequence modelling using Bayesian inference

In order to integrate and utilize all the information from the available dataset and well-defined stratigraphy, we built a Bayesian age sequence model using ChronoModel v. 2.0 software (Lanos and Dufresne, 2019). In doing so we aimed to: (i) develop a robust, comprehensive and up-to-date eruptive chronology for the MSg tephra beds; (ii) realistically estimate the ages and quantify age uncertainties for those tephras that have not been directly radiometrically dated; and (iii) test the sensitivity of the Bayesian model to different types of input data.

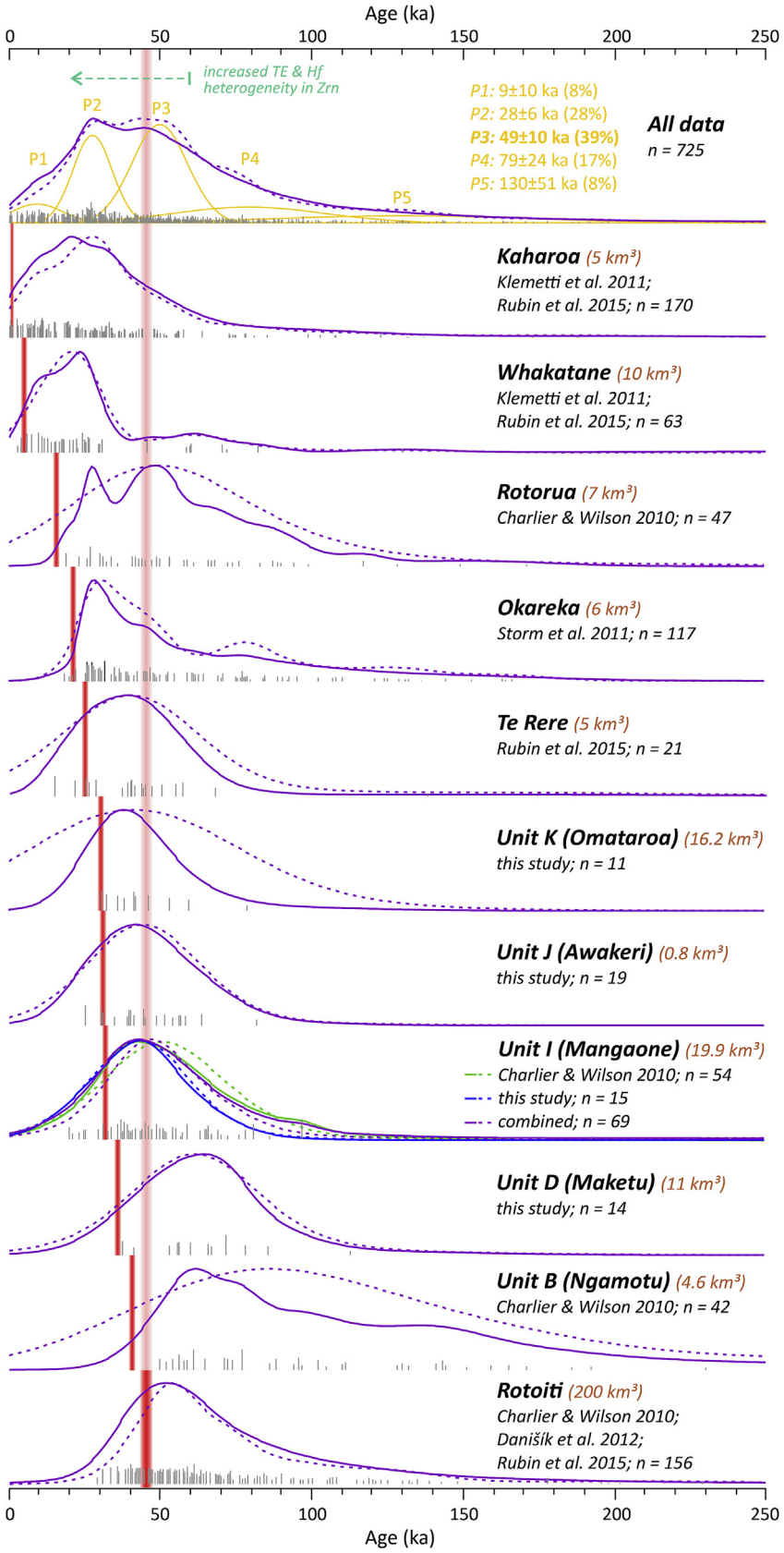

Fig. 10. Compilation of available U–Th zircon crystallization ages for Rotoiti and post-Rotoiti eruptions from the OVC. Kernel density estimates (KDE; dashed lines) and probability density function (PDF, solid lines) curves were constructed in DensityPlotter v.7.3 (Vermeesch, 2012); data-points represented by grey tick marks; eruption ages represented by vertical red bars. Major components identified using DensityPlotter v.7.3 are shown in the top panel; identified age populations (P1–5) are represented by Gaussian curves as well as described by age ± standard deviation (in ka) and fraction (in %); non-consolidated volumes in km^3 (brown numbers) after Jurado-Chichay and Walker (2000) and Wilson et al.

The schematic structure of the model was described in Section 3.3. In brief, a sequence of 14 events is defined, representing 13 MSg tephras and the Tahuna tephra in stratigraphic order as defined in Smith et al. (2005) and Wilson et al. (2009) (Table 1). The sequence is bracketed from the bottom by the Rotoiti and Earthquake Flat events with assigned eruption ages of 45.2 ± 1.65 and 45.2 ± 1.45 ka BP (Danišík et al., 2012), respectively, and by the Oruanui/Kawakawa event at the top with an eruption age of 25.4 ± 0.2 cal ka BP (Vandergoes et al., 2013; see also Dunbar et al., 2017) (Supplementary Figure S1). Three models with different input parameters were constrained as follows (Supplementary Table S1): Model 1 took into account only ^{14}C data that we considered to be of the highest quality available for each tephra as specified in Table 2. These data were complemented in Model 2 with the ZDD data. In Model 3 we considered all ^{14}C data, regardless of quality, and the ZDD data.

Results presented in Fig. 8 show that the posterior eruption ages and uncertainties predicted by the three models are almost identical. Only a subtle difference in age uncertainty of <0.5 ka is present in the modelled ages for Units I (Mangaone), J (Awakeri), and K (Omataroa), with Model 3 predicting the lowest, and Model 2 the highest, uncertainties (Fig. 8). The excellent overall similarity of the posterior eruption ages predicted by the three models demonstrates that our modelling approach based on hierarchical Bayesian inference is not significantly affected by the presence of outliers and offers a robust means to estimate the chronology of eruption events based on multiple geochronological data combined with a priori information from stratigraphic superpositioning.

For interpretation purposes, we adopt the posterior distributions of Model 2, based on the highest quality ^{14}C and ZDD data, as our best estimates for eruption ages for all the MSg tephras (Fig. 9). These results constrain the duration of MSg activity between $42.7^{+3.7}_{-3.5}$ and $30.6^{+0.6}_{-1.5}$ ka BP (MAP ± 95% HPD) based on posterior distributions for Unit A and Unit L, respectively. The beginning of MSg activity is of particular importance here because this age was only indirectly estimated based on the age of underlying Rotoiti/Rotoehu deposits, which for several decades had been considered to be in the 64–61 ka range (Wilson et al., 1992, 2007). Nevertheless, some authors estimated the onset of MSg activity to have taken place ~44–43 ka (no uncertainties provided; Jurado-Chichay and Walker, 2000; Wilson et al., 2009; Leonard et al., 2010). Our modelled onset age (~43 ka) implies that several volcanic deposits that occur in stratigraphic juxtapositions between the Rotoiti/Rotoehu and MSg tephras are younger than previously considered (e.g., six un-named eruptives from Taupo caldera, and the Forest Rd dome tephra from Maroa caldera, reported in Wilson et al., 2009, and the Otake, Waihora, and Tihoi tephras, reported in Vucetich and Howorth, 1976; Froggatt and Lowe, 1990; Wilson et al., 2009). Our results also suggest a much shorter period of quiescence between the Rotoiti/Rotoehu and MSg events, lasting no more than a few thousand years, which has implications for calculation of magma eruption rates for the OVC. Finally, in addition to Unit A ($42.7^{+3.7}_{-3.5}$ ka BP), based on the new data herein, we propose the following ages and uncertainties for previously undated MSg tephras: Unit B (Ngamotu) $39.6^{+4.5}_{-1.9}$; Unit C1 (Pupuwharau) $37.7^{+1.5}_{-1.4}$; Unit C2 (Pongakawa) $36.6^{+1.6}_{-1.0}$; Unit G $33.8^{+1.7}_{-2.0}$; and Unit H $31.8^{+2.6}_{-0.8}$ka BP (MAP ± 95% HPD).

5.3. Implications for magmatic evolution of the Okataina Volcanic Centre

In addition to eruptive chronology, ZDD may provide insights into the dynamics of magmatic systems via direct provision of zircon U–Th crystallization ages (Schmitt, 2011). Although our dataset for the four dated tephras is of smaller size (n = 59) and lacks information on trace element or isotopic composition of zircon, the U–Th age spectra allow us to identify some features that may further improve understanding of the dynamics of the OVC magma reservoir.

Model age spectra for all four tephras are broad and contain ages that record a crystallization age that is ≥30 kyrs older than the eruption age (Figs. 6 and 10). This finding is consistent with the interpretation that the OVC zircons were most likely extracted from a crystal mush that may have existed at depth long before the eruptions (Storm et al., 2011). The presence of >45 ka crystallization ages in all dated MSg tephras confirms that the climactic pre-MSg Rotoiti eruption at ca. 45 ka did not exhaustively depleted the OVC crystal reservoir and that a significant number of zircon crystals survived this extraction event (Storm et al., 2011).

The model age spectrum for Unit D (Maketu) is broad and unimodal with a dominant peak at ca. 62 ka. The majority of ages are older than the 45 ka caldera-forming Rotoiti eruption, documenting that zircon crystallized from at least ca. 110 ka up until eruption at ca. 36 ka, and that most were formed prior to the Rotoiti event (Fig. 10). In contrast to that of Unit D (Maketu), the model age spectra for Units I (Mangaone), J (Awakeri), and K (Omataroa) are narrower and unimodal, with dominant peaks at ca. 41–45 ka, documenting that these zircon grains not only crystallized from ca. 90 ka until their eruption at ca. 30–32 ka, but also that zircon crystallization peaked at ca. 41–45 ka, shortly before, during, or shortly after the Rotoiti eruption event (Fig. 10).

Similar patterns can be seen in the zircon U–Th age spectra reported by Charlier and Wilson (2010) for Unit B (Ngamotu) and Unit I (Mangaone). The U–Th age spectrum for Unit B (Ngamotu) (Charlier and Wilson, 2010) is similar to that obtained in this work for Unit D (Maketu), namely broad, more complex, and with a major population (ca. 70 ka) older than the Rotoiti event. Notably, both spectra are similar to the U–Th model age spectrum for Rotoiti zircons (Fig. 10). These data suggest that Unit B (Ngamotu) and Unit D (Maketu) eruptions sampled zircon crystals from a reservoir that crystallized and stored zircons long before the Rotoiti eruption. The zircon U–Th age spectrum for Unit I (Mangaone) reported by Charlier and Wilson (2010) has a dominant peak at ca. 45 ka, coeval with the Rotoiti event, and similar to the spectra for Units I (Mangaone), J (Awakeri), and K (Omataroa) from our work, suggesting that although some zircon crystals were sourced from a long-lived part of the magma reservoir, the majority formed shortly before, during, or shortly after the Rotoiti event. From this inference we suggest that Units I (Mangaone), J (Awakeri), and K (Omataroa) eruptions tapped magma from the same domain of the reservoir and that this domain was geochronologically distinct from those of Unit B (Ngamotu) and Unit D (Maketu).

The difference in U–Th age patterns between Old MSg and Young MSg tephras, first observed by Charlier and Wilson (2010) and corroborated and complemented here, is consistent with the well-documented shift in composition, temperature, and vent

(2009). The age for the caldera-forming Rotoiti eruption is projected across all the post-Rotoiti eruptions. Note that Unit I (Mangaone) eruption was the first one to provide the majority of zircon crystals that formed during or after the Rotoiti eruption, whereas Unit B (Ngamotu) and Unit D (Maketu) sourced mostly pre-Rotoiti zircon crystals. Also note that the majority of zircon crystals erupted from OVC in the past 45 kyrs formed shortly before, during, and shortly after the Rotoiti event as suggested by the major age population of 49 ± 10 ka comprising 39% of all dated crystals. This finding is consistent with the onset of increasing diversification of trace element and isotopic compositions in OVC zircon starting at ca. 60 ka (Rubin et al., 2016) and major 'reorganization' of the OVC caldera during and after the Rotoiti event (Shane et al., 2005a,b; Smith et al., 2005; Storm et al., 2014; Rubin et al., 2016). (For interpretation of the references to colour in this figure legend, the reader is referred to the Web version of this article.)

location within the MSg (Jurado-Chichay and Walker, 2000; Smith et al., 2002, 2005). Whereas Unit B (Ngamotu) and Unit D (Maketu) tephras are low-SiO_2 rhyolite and rhyodacite, respectively, erupted at 935 °C presumably from the south western (Unit B (Ngamotu)) and north-central (Unit D (Maketu)) parts of the OVC, Units I (Mangaone), J (Awakeri), and K (Omataroa) are high-SiO_2 rhyolites that were erupted at lower temperatures (755–828 °C) from the eastern margin of the OVC (Jurado-Chichay and Walker, 2000; Smith et al., 2002, 2005). These changes show that MSg tephras were derived from compositionally and geographically distinct domains below the volcano, progressing to more evolved, cooler, and possibly shallower magmas (Jurado-Chichay and Walker, 2000; Smith et al., 2002, 2005), and have been attributed to 'reorganization' of the OVC magma reservoir following the caldera collapse at ca. 45 ka (Shane et al., 2005a; Klemetti et al., 2011; Storm et al., 2014). Based on patterns in trace element and Hf isotopic data collected from Rotoiti and post-MSg tephras (Klemetti et al., 2011; Storm et al., 2014; Rubin et al., 2016), it has been shown that the reorganization resulted in less effective interconnectedness within the OVC reservoir and its segregation into chemically distinct melt pockets which did not exist prior to caldera collapse (Rubin et al., 2016). Similarly, Cole et al. (2014) suggested from analyses of Unit I (Mangaone) (referred to as Kawerau Ignimbrite) that it reflected two discrete magmas, hence providing evidence for the existence of multiple discrete magmas in the OVC. Our geochronological results confirm the model of chemically distinct melt pockets and, further, suggest that the degree of interconnectedness within the OVC magmatic system decreased during the MSg eruption period, most likely between the eruption of Unit D (Maketu) and Unit I (Mangaone).

Our new data complement the existing dataset of U–Th ages reported for other major eruptions of the OVC (Charlier and Wilson, 2010; Klemetti et al., 2011; Storm et al., 2011; Danišík et al., 2012; Rubin et al., 2016). We acknowledge that previous studies conducted U–Th SIMS analyses on different parts of zircon crystals (e.g., rim analysis on surfaces, rim analysis on sectioned and polished crystal surfaces, core analysis on sectioned and polished crystal surfaces), and therefore the U–Th ages may record different stages of crystal growth and not necessarily the last stage of zircon crystallization. Nevertheless, the data can be used as a proxy to identify periods of zircon crystallization.

The age spectrum of all currently available U–Th ages for the OVC (Fig. 10) confirms quasi-continuous zircon crystallization under OVC since at least ca. 250 ka (Storm et al., 2011; Klemetti et al., 2011). Principle component analysis using the 'auto' mixture model implemented in DensityPlotter 7.3 (Vermeesch, 2012) revealed two dominant age populations at 49 ± 10 ka (1 standard deviation; 39% fraction) and 28 ± 6 ka (1 standard deviation; 28% fraction), and three subordinate components at 9 ± 10 ka (1 standard deviation; 8% fraction), 79 ± 24 ka (17% fraction), and 130 ± 51 ka (8% fraction). The dominant 49 ± 10 ka age population suggests that the majority of zircon crystallized prior to, during, and after the caldera-forming Rotoiti eruption. This result is consistent with an observed increase in the variability of zircon isotopic and trace element compositions which started after ca. 60 ka and is most pronounced in post-Rotoiti zircon crystallized at 40–20 ka (Storm et al., 2014; Rubin et al., 2016). It is notable that the latter age range is consistent with the second dominant population of 28 ± 6 ka. It has been hypothesised that the change of reservoir behaviour at ca. 60 ka was related to increased rate of extension and/or changes in thermal flux at the OVC (Smith et al., 2005; Rubin et al., 2016).

6. Conclusions and outlook

A well-established sequence of Mangaone Subgroup tephras from the Okataina Volcanic Centre (New Zealand) was used as a natural laboratory to conduct a cross-validation experiment in which we tested the accuracy of eruption ages derived using ZDD against published and new ^{14}C eruption ages. ZDD eruption ages of 36.1 ± 4.4, 31.5 ± 5.2, 30.9 ± 5.6, 31.2 ± 4.4 ka BP for Units D (Maketu), I (Mangaone), J (Awakeri), K (Omataroa), respectively, are statistically indistinguishable from optimum ^{14}C-based eruption ages on the same or stratigraphically bracketing tephras. These results demonstrate the feasibility of ZDD to date eruption ages accurately.

The relatively low precision of our ZDD eruption ages (12–18% age uncertainties at 2σ) stems primarily from the low U content in dated zircon, relatively young eruption age, and low number (i.e., 7–9) of single grain replicates analysed per sample. The precision could be lowered to <10% (2σ) by analysing more (~20) replicates. Although the number of replicates will always be sample specific and dependent on several factors (eruption age, crystal availability, U–Th content, capacity of analytical facilities, budget), in general we tentatively recommend analysing 7–20 crystals per sample to achieve reasonable ZDD precision.

U–Th zircon crystallization data revealed that the majority of zircon crystals from Unit D (Maketu) crystallized prior to the caldera-forming Rotoiti (Rotoehu) eruption at ca. 45 ka. In contrast, the majority of zircon from Units I (Mangaone), J (Awakeri), and K (Omataroa) crystallized during or shortly after the Rotoiti eruption and were likely derived from a distinct reservoir domain. This age difference is consistent with the change in composition, temperature, and vent location for Old and Young MSg tephras, confirming decreasing interconnectedness within the OVC reservoir, and providing further geochronological evidence for the complexity of the OVC magma reservoir.

Based on the new ZDD ages, and new and published ^{14}C data, we present a revised geochronology for all 13 MSg tephras determined by a Bayesian age sequence model built in ChronoModel v. 2.0 software. The revised eruption ages (±95% HPD regions) for the MSg tephras, and the Tahuna tephra, are: $42.7^{+3.7}_{-3.5}$(Unit A), $39.6^{+4.5}_{-1.9}$ (Unit B (Ngamotu)), $38.4^{+1.7}_{-1.4}$(Tahuna), $37.7^{+1.5}_{-1.4}$(Unit C1 (Pupuwharau)), $36.6^{+1.6}_{-1.0}$(Unit C2 (Pongakawa)), $36.1^{+0.9}_{-0.8}$ (Unit D), $35.6^{+0.8}_{-1.0}$ (Unit E), $35.2^{+1.0}_{-2.0}$ (Unit F), $33.8^{+1.7}_{-2.0}$ (Unit G), $31.8^{+2.6}_{-0.8}$ (Unit H), $31.1^{+1.0}_{-0.4}$ (Unit I), $31.0^{+0.9}_{-0.8}$ (Unit J), $30.8^{+0.8}_{-1.0}$ (Unit K), and $30.6^{+0.6}_{-1.5}$ ka BP (Unit L). These results refine the existing eruptive geochronology in New Zealand by constraining the beginning of the MSg phase to $42.7^{+3.7}_{-3.5}$ cal ka (Unit A), and by providing comprehensive estimates of eruption ages and age uncertainties for MSg units that have not been directly dated previously. The frequency of eruption for the entire MSg tephra sequence of 13 episodes, emplaced over an interval of ~12,100 cal years, is every ~930 years on average.

Our study demonstrates the efficacy of ZDD to yield accurate eruption ages and highlights its potential for dating eruption events considerably younger than 1 Myr, which are challenging to date by other geochronological methods. While ZDD can be applied to numerous silicic and other zircon-producing volcanic centres on Earth, we suggest that our study may provide an impetus for wider and systematic application of ZDD in New Zealand. There is an exceptionally well-documented record of numerous regionally important, yet undated, silicic volcanic deposits aged from ca. 50 ka to 1 Ma in New Zealand, many of which would be excellent targets for development of a high-precision tephrostratigraphic framework extending well beyond the conventional limits of ^{14}C.

Declaration of competing interest

The authors declare that they have no known competing

financial interests or personal relationships that could have appeared to influence the work reported in this paper.

Acknowledgements

MD was supported by the AuScope NCRIS2 program, Australian Research Council (ARC) Discovery funding scheme (DP160102427) and Curtin Research Fellowship. Part of this research was undertaken using the SEM instrumentation (ARC LE0775553) at the John de Laeter Centre, Curtin University. We acknowledge the help of A.S. Kumara, A. Frew, B. Ware, and E. Miller with mineral separation, zircon dissolution, solution ICP-MS analyses and SEM imaging, and K. Holt for generating an early version of Table 2. MD thanks I. Dunkl for sharing PepiFLEX software for ICP-MS data reduction, P. Lanos for providing guidance on Bayesian modelling in ChronoModel, and M. Meredith for writing an R code for Bayesian analysis for comparing two groups. DJL acknowledges the New Zealand Marsden Fund *Te Pūta Rangahau a Marsden* for supporting tephra-paleosol research in the Bay of Plenty area for the project "New Views from old soils: testing the reconstruction of environmental and climatic change using genetic signals preserved in buried paleosols" (10-UOW-056). The paper is an output of the Commission on Tephrochronology (COT) of the International Association of Volcanism and Chemistry of the Earth's Interior (IAVCEI). Two anonymous reviewers and G. Zanchetta (editor) are thanked for positive and helpful evaluations.

Appendix A. Supplementary data

Supplementary data to this article can be found online at https://doi.org/10.1016/j.quascirev.2020.106517.

References

Berryman, K.R., 1992. A stratigraphic age of Rotoehu Ash and late Pleistocene climate interpretation based on marine terrace chronology, Mahia Peninsula, North Island, New Zealand. N. Z. J. Geol. Geophys. 35, 1–7.
Blondes, M.S., Reiners, P.W., Edwards, B.R., Biscontini, A., 2007. Dating young basalt eruptions by (U-Th)/He on xenolithic zircons. Geology 35 (1), 17–20.
Boehnke, P., Watson, E.B., Trail, D., Harrison, T.M., Schmitt, A.K., 2013. Zircon saturation re-revisited. Chem. Geol. 351, 324–334.
Briggs, R.M., Lowe, D.J., Esler, W.R., Smith, R.T., Henry, M.A.C., Wehrmann, H., Manning, D.A., 2006. Geology of the Maketu Area, Bay of Plenty, North Island, New Zealand - Sheet V14 1:50 000, 26. Department of Earth Sciences, University of Waikato, Occasional Report, pp. 1–44.
Bronk Ramsey, C., 2009. Bayesian analysis of radiocarbon dates. Radiocarbon 51, 337–360.
Burgess, S.D., Coble, M.A., Vazquez, J.A., Coombs, M.L., Wallace, K.L., 2019. On the eruption age and provenance of the Old Crow tephra. Quat. Sci. Rev. 207, 64–79.
Charlier, B.L.A., Wilson, C.J.N., 2010. Chronology and evolution of caldera-forming and post-caldera magma systems at Okataina Volcano, New Zealand from zircon U–Th model-age spectra. J. Petrol. 51 (5), 1121–1141.
Charlier, B.L., Peate, D.W., Wilson, C.J., Lowenstern, J.B., Storey, M., Brown, S.J., 2003. Crystallisation ages in coeval silicic magma bodies: ^{238}U–^{230}Th disequilibrium evidence from the Rotoiti and Earthquake Flat eruption deposits, Taupo Volcanic Zone, New Zealand. Earth Planet Sci. Lett. 206 (3–4), 441–457.
Cherniak, D.J., Watson, E.B., 2001. Pb diffusion in zircon. Chem. Geol. 172 (1), 5–24.
Chesner, C.A., Barbee, O.A., McIntosh, W.C., 2020. The enigmatic origin and emplacement of the Samosir Island lava domes, Toba Caldera, Sumatra, Indonesia. Bull. Volcanol. 82 (3), 1–20.
Coble, M.A., Burgess, S.D., Klemetti, E.W., 2017. New zircon (U-Th)/He and U/Pb eruption age for the Rockland tephra, western USA. Quat. Sci. Rev. 172, 109–117.
Cole, J.W., Spinks, K.D., Deering, C.D., Nairn, I.A., Leonard, G.S., 2010. Volcanic and structural evolution of the Okataina Volcanic Centre; dominantly silicic volcanism associated with the Taupo Rift, New Zealand. J. Volcanol. Geoth. Res. 190, 123–135.
Cole, J.W., Deering, C.D., Nairn R.M., Burt, Sewell, S., Shane, P.A.R., Matthews, N.E., 2014. Okataina Volcanic Centre, Taupo Volcanic Zone, New Zealand: a review of volcanism and synchronous pluton development in an active, dominantly silicic caldera system. Earth-Sci. Rev. 128, 1–17.
Danišík, M., McInnes, B.I., Kirkland, C.L., McDonald, B.J., Evans, N.J., Becker, T., 2017b. Seeing is believing: visualization of He distribution in zircon and implications for thermal history reconstruction on single crystals. Science Advances 3 (2), e1601121.
Danišík, M., Schmitt, A.K., Stockli, D.F., Lovera, O.M., Dunkl, I., Evans, N.J., 2017a. Application of combined U-Th-disequilibrium/U-Pb and (U-Th)/He zircon dating to tephrochronology. Quat. Geochronol. 40, 23–32.
Danišík, M., Shane, P., Schmitt, A.K., Hogg, A., Santos, G.M., Storm, S., Evans, N.J., Fifield, L.K., Lindsay, J.M., 2012. Re-anchoring the late Pleistocene tephrochronology of New Zealand based on concordant radiocarbon ages and combined $^{238}U/^{230}Th$ disequilibrium and (U–Th)/He zircon ages. Earth Planet Sci. Lett. 349–350, 240–250.
Dunbar, N.W., Iverson, N.A., Van Eaton, A.R., Sigl, M., Alloway, B.V., Kurbatov, A.V., Mastin, L.G., McConnell, J.R., Wilson, C.J.N., 2017. New Zealand supereruption provides time marker for the Last Glacial Maximum in Antarctica. Sci. Rep. 7, 12238.
Evans, N.J., Byrne, J.P., Keegan, J.T., Dotter, L.E., 2005. Determination of uranium and thorium in zircon, apatite, and fluorite: application to laser (U–Th)/He thermochronology. J. Anal. Chem. 60 (12), 1159–1165.
Farley, K.A., Kohn, B.P., Pillans, B., 2002. The effects of secular disequilibrium on (U–Th)/He systematics and dating of Quaternary volcanic zircon and apatite. Earth Planet Sci. Lett. 201, 117–125.
Farley, K.A., Wolf, R.A., Silver, L.T., 1996. The effects of long alpha-stopping distances on (U-Th)/He ages. Geochem. Cosmochim. Acta 60, 4223–4229.
Flude, S., Storey, M., 2016. $^{40}Ar/^{39}Ar$ age of the Rotoiti Breccia and Rotoehu Ash, Okataina Volcanic Complex, New Zealand, and identification of heterogeneously distributed excess ^{40}Ar in supercooled crystals. Quat. Geochronol. 33, 13–23.
Friedrichs, B., Schmitt, A.K., McGee, L., Turner, S., 2020. U-Th whole rock data and high spatial resolution U-Th disequilibrium and U-Pb zircon ages of Mt. Erciyes and Mt. Hasan Quaternary stratovolcanic complexes (Central Anatolia). Data in Brief 29, 105113.
Froggatt, P.C., Lowe, D.J., 1990. A review of late Quaternary silicic and some other tephra formations from New Zealand: their stratigraphy, nomenclature, distribution, volume and age. N. Z. J. Geol. Geophys. 33, 89–109.
Gelman, A., Carlin, J.B., Stern, H.S., Dunson, D.B., Vehtari, A., Rubin, D.B., 2013. In: Bayesian Data Analysis. Chapman and Hall/CRC, pp. 1–675.
Gençalioğlu-Kuşcu, G., Uslular, G., Danišík, M., Koppers, A., Miggins, D.P., Friedrichs, B., Schmitt, A.K., 2020. U–Th disequilibrium, (U–Th)/He and $^{40}Ar/^{39}Ar$ geochronology of distal Nisyros Kyra tephra deposits on Datça peninsula (SW Anatolia). Quat. Geochronol. 55 (101033), 1–13.
Grant-Taylor, T.L., Rafter, T.A., 1971. New Zealand radiocarbon age measurements — 6. N. Z. J. Geol. Geophys. 14, 364–402.
Harangi, S., Lukács, R., Schmitt, A.K., Dunkl, I., Molnár, K., Kiss, B., Seghedi, I., Novothny, Á., Molnár, M., 2015. Constraints on the timing of Quaternary volcanism and duration of magma residence at Ciomadul volcano, east-central Europe, from combined U-Th/He and U-Th zircon geochronology. J. Volcanol. Geoth. Res. 301, 66–80.
Hodder, A.P.W., Green, B.E., Lowe, D.J., 1990. A two-stage model for the formation of clay minerals from tephra derived volcanic glass. Clay Miner. 25, 313–327.
Hogg, A.G., McCraw, J.D., 1983. Late Quaternary tephras of Coromandel Peninsula, North Island, New Zealand: a mixed peralkaline and calcalkaline tephra sequence. N. Z. J. Geol. Geophys. 26, 163–187.
Hogg, A.G., Fifield, L.K., Palmer, J.G., Turney, C.S., Galbraith, R., 2007. Robust radiocarbon dating of wood samples by high-sensitivity liquid scintillation spectroscopy in the 50–70 kyr age range. Radiocarbon 49 (2), 379–391.
Hogg, A.G., Hua, Q., Blackwell, P.G., Niu, M., Buck, C.E., Guilderson, T.P., Heaton, T.J., Palmer, J.G., Reimer, P.J., Reimer, R.W., Turney, C.S.M., Zimmerman, S.R.H., 2013. SHCal13 Southern Hemisphere calibration, 0–50,000 years cal BP. Radiocarbon 55 (4), 1889–1903.
Hogg, A.G., Wilson, C.J.N., Lowe, D.J., Turney, C.S.M., White, P., Lorrey, A.M., Manning, S.W., Palmer, J.G., Bury, S., Brown, J., Southon, J., Petchey, F., 2019. Wiggle-match radiocarbon dating of the Taupo eruption. Nat. Commun. 10, 4669.
Hopkins, J.L., Wilson, C.J., Millet, M.A., Leonard, G.S., Timm, C., McGee, L.E., Smith, I.E.M., Smith, E.G., 2017. Multi-criteria correlation of tephra deposits to source centres applied in the Auckland Volcanic Field, New Zealand. Bull. Volcanol. 79 (7), 55. https://doi.org/10.1007/s00445-017-1131-y.
Hourigan, J.K., Reiners, P.W., Brandon, M.T., 2005. U-Th zonation dependent alpha-ejection in (U-Th)/He chronometry, Part I: Theory. Geochem. Cosmochim. Acta 69, 3349–3365.
Houghton, B.F., Weaver, S.D., Wilson, C.J.N., Lanphere, M.A., 1992. Evolution of a Quaternary peralkaline volcano: Mayor Island, New Zealand. J. Volcanol. Geoth. Res. 51, 217–236.
Howorth, R., 1975. New formations of late Pleistocene tephras from the Okataina Volcanic Centre, New Zealand. N. Z. J. Geol. Geophys. 18 (5), 683–712.
Howorth, R., 1981. Editorial. In: Howorth, R., et al. (Eds.), Proceedings of Tephra Workshop.. Geology Department Victoria University of Wellington Publication, 20, pp. 1–4.
Ito, H., Danišík, M., 2020. Dating late Quaternary events by the combined U-Pb LA-ICP-MS and (U-Th)/He dating of zircon: a case study on Omachi Tephra suite (central Japan). Terra. Nova 32 (2), 134–140.
Jurado-Chichay, Z., Walker, G.P.L., 2000. Stratigraphy and dispersal of the Mangaone subgroup pyroclastic deposits, Okataina volcanic centre, New Zealand. J. Volcanol. Geoth. Res. 104 (1–4), 319–380.
Jurado-Chichay, Z., Walker, G.P.L., 2001a. The intensity and magnitude of the Mangaone subgroup plinian eruptions from Okataina Volcanic Centre, New Zealand. J. Volcanol. Geoth. Res. 111, 219–237.
Jurado-Chichay, Z., Walker, G.P.L., 2001b. Variability of plinian fall deposits:

examples from Okataina Volcanic Centre, New Zealand. J. Volcanol. Geoth. Res. 111, 239–263.
Kirkland, C.L., Danišík, M., Marsden, R., Piilonen, P., Barham, M., Sutherland, L., 2020. Dating young zircon: a case study from Southeast Asian megacrysts. Geochem. Cosmochim. Acta 274, 1–19.
Klemetti, E.W., Deering, C.D., Cooper, K.M., Roeske, S.M., 2011. Magmatic perturbations in the Okataina Volcanic Complex, New Zealand at thousand-year timescales recorded in single zircon crystals. Earth Planet Sci. Lett. 305 (1–2), 185–194.
Kruschke, J.K., 2013. Bayesian estimation supersedes the t test. J. Exp. Psychol. Gen. 142 (2), 573–603.
Lanos, P., Philippe, A., 2017. Hierarchical Bayesian modeling for combining dates in archaeological context. J. Soc. Fr. Stat. 158, 72–88.
Lanos, P., Dufresne, P., 2019. ChronoModel Version 2.0: User Manual. Available from: http://www.chronomodel.com.
Lanos, P., Philippe, A., 2018. Event date model: a robust Bayesian tool for chronology building. Communications for Statistical Applications and Methods, Korean Statistical Society (KSS) /Korean International Statistical Society (KISS) 25 (2), 131–157.
Leonard, G.S., Begg, J.G., Wilson, C.J.N., 2010. Geology of the Rotorua Area: Scale 1: 250,000. Institute of Geological and Nuclear Sciences 1: 250,000 Geological Map 5. 1 Sheet. Institute of Geological and Nuclear Sciences, Lower Hutt, pp. 1–99.
Lian, O.B., Shane, P.A., 2000. Optical dating of paleosols bracketing the widespread Rotoehu tephra, North Island, New Zealand. Quat. Sci. Rev. 19 (16), 1649–1662.
Loame, R.C., Villamor, P., Lowe, D.J., Milicich, S.D., Pittari, A., Barker, S.L., Rae, A., Gómez-Vasconcelos, M.G., Martinez-Martos, M., Ries, W.F., 2019. Using paleoseismology and tephrochronology to reconstruct fault rupturing and hydrothermal activity since c. 40 ka in Taupo Rift, New Zealand. Quat. Int. 500, 52–70.
Lowe, D.J., Percival, H.J., 1993. Clay mineralogy of tephras and associated paleosols and soils, and hydrothermal deposits. In: North Island. Guide Book for New Zealand Pre-conference Field Trip FI, 10th International Clay Conference, Adelaide, Australia, p. 110.
Lowe, D.J., Hogg, A.G., 1995. Age of the Rotoehu ash. N. Z. J. Geol. Geophys. 38, 399–402.
Ludwig, K.R., 2012. User's Manual for Isoplot 3.75: A Geochronological Toolkit for Microsoft Excel, vol. 5. Berkeley Geochronology Center Special Publication, p. 75.
Mark, D.F., Renne, P.R., Dymock, R.C., Smith, V.C., Simon, J.I., Morgan, L.E., Staff, R.A., Ellis, B.S., Pearce, N.J., 2017. High-precision $^{40}Ar/^{39}Ar$ dating of Pleistocene tuffs and temporal anchoring of the Matuyama-Brunhes boundary. Quat. Geochronol. 39, 1–23.
McGlone, M.S., Howorth, R., Pullar, W.A., 1984. Late Pleistocene stratigraphy, vegetation and climate of the Bay of Plenty and Gisborne regions, New Zealand. N. Z. J. Geol. Geophys. 27, 327–350.
Molloy, C., Shane, P., Augustinus, P., 2009. Eruption recurrence rates in a basaltic volcanic field based on tephra layers in maar sediments: implications for hazards in the Auckland Volcanic Field. Geol. Soc. Am. Bull. 121 (11–12), 1666–1677.
Molnár, K., Harangi, S., Lukács, R., Dunkl, I., Schmitt, A.K., Kiss, B., Garamhegyi, T., Seghedi, I., 2018. The onset of the volcanism in the Ciomadul Volcanic Dome Complex (eastern Carpathians): eruption chronology and magma type variation. J. Volcanol. Geoth. Res. 354, 39–56.
Mucek, A.E., Danišík, M., de Silva, S.L., Schmitt, A.K., Pratomo, I., Coble, M.A., 2017. Post-supereruption recovery at toba caldera. Nat. Commun. 8 (1), 1–9.
Nairn, I.A., 1972. Rotoehu Ash and Rotoiti Breccia Formation, Taupo Volcanic Zone, New Zealand. N. Z. J. Geol. Geophys. 15, 251–261.
Nairn, I., 1981. Some studies of the geology, volcanic history, and geothermal resources of the Okataina Volcanic Centre, Taupo Volcanic Zone, New Zealand. Unpublished Ph.D. thesis, lodged in the Library, Victoria University of Wellington, Wellington.
Nairn, I.A., 1989. Sheet V16AC Tarawera – Geological Map of New Zealand 1:50 000. New Zealand Department of Scientific and Industrial Research, Wellington.
Nairn, I.A., 2002. Geology of the Okataina Volcanic Centre, Scale 1: 50000. Institute of Geological and Nuclear Sciences, Lower Hutt, New Zealand.
Newnham, R.M., Lowe, D.J., Green, J.D., Turner, G.M., Harper, M.A., McGlone, M.S., Stout, S.L., Horie, S., Froggatt, P.C., 2004. A discontinuous ca. 80 ka record of Late Quaternary environmental change from Lake Omapere, Northland, New Zealand. Palaeogeogr. Palaeoclimatol. Palaeoecol. 207, 165–198.
Nilsson, A., Muscheler, R., Snowball, I., Aldahan, A., Possnert, G., Augustinus, P., Atkin, D., Stephens, T., 2011. Multi-proxy identification of the Laschamp geomagnetic field excursion in Lake Pupuke, New Zealand. Earth Planet Sci. Lett. 311, 155–164. https://doi.org/10.1016/j.epsl.2011.08.050.
Paces, J.B., Miller Jr., J.D., 1993. Precise U-Pb ages of Duluth Complex and related mafic intrusions, northeastern Minnesota: geochronological insights to physical, petrogenetic, paleomagnetic, and tectonomagnetic processes associated with the 1.1 Ga Midcontinent Rift system. J. Geophys. Res. 98 (B8), 13997–14013.
Peti, L., Augustinus, P.C., 2019. Stratigraphy and sedimentology of the Orakei maar lake sediment sequence (Auckland Volcanic Field, New Zealand). Sci. Drill. 25, 47–56.
Pillans, B., Wright, I., 1992. Late Quaternary tephrostratigraphy from the southern Havre Trough-Bay of Plenty, northeast New Zealand. N. Z. J. Geol. Geophys. 35 (2), 129–143.
Pullar, W.A., Heine, J.C., 1971. Ages, inferred from ^{14}C dates, of some tephra and other deposits from Rotorua, Taupo, Bay of Plenty, Gisborne, and Hawke's Bay districts. In: Proceedings, Radiocarbon Users' Conference, 17-18 August 1971, Lower Hutt, New Zealand, pp. 117–138.
Pullar, W.A., Birrell, K.S., Heine, J.C., 1973. Named tephras and tephra formations occurring in the central North Island, with notes on derived soils and buried paleosols. N. Z. J. Geol. Geophys. 16 (3), 497–518.
Reiners, P.W., Spell, T.L., Nicolescu, S., Zanetti, K.A., 2004. Zircon (U-Th)/He thermochronometry: He diffusion and comparisons with $^{40}Ar/^{39}Ar$ dating. Geochem. Cosmochim. Acta 68, 1857–1887.
Reiners, P.W., 2005. Zircon (U-Th)/He thermochronometry. In: Reiners, P.W., Ehlers, T.A. (Eds.), Thermochronology, Reviews in Mineralogy and Geochemistry, vol. 58, pp. 151–176.
Rubin, A.E., Cooper, K.M., Leever, M., Wimpenny, J., Deering, C., Rooney, T., Gravley, D., Yin, Q.-Z., 2016. Changes in magma storage conditions following caldera collapse at Okataina Volcanic Center, New Zealand. Contrib. Mineral. Petrol. 171, 1–18.
Sakata, S., Hirakawa, S., Iwano, H., Danhara, T., Guillong, M., Hirata, T., 2017. A new approach for constraining the magnitude of initial disequilibrium in Quaternary zircons by coupled uranium and thorium decay series dating. Quat. Geochronol. 38, 1–12. https://doi.org/10.1016/j.quageo.2016.11.002.
Santos, G.M., Bird, M.I., Pillans, B., Fifield, L.K., Alloway, B.V., Chappell, J., Hausladen, P.A., Arneth, A., 2001. Radiocarbon dating of wood using different pretreatment procedures: application to the chronology of Rotoehu Ash, New Zealand. Radiocarbon 43 (2A), 239–248.
Schmitt, A.K., Stockli, D.F., Lindsay, J.M., Robertson, R., Lovera, O.M., Kislitsyn, R., 2010a. Episodic growth and homogenization of plutonic roots in arc volcanoes from combined U-Th and (U-Th)/He zircon dating. Earth Planet Sci. Lett. 295, 91–103.
Schmitt, A.K., Stockli, D.F., Niedermann, S., Lovera, O.M., Hausback, B.P., 2010b. Eruption ages of Las Tres Vírgenes volcano (Baja California): a tale of two helium isotopes. Quat. Geochronol. 5, 503–511.
Schmitt, A.K., 2007. Ion microprobe analysis of $(^{231}Pa)/(^{235}U)$ and an appraisal of protactinium partitioning in igneous zircon. Am. Mineral. 92 (4), 691–694.
Schmitt, A.K., 2011. Uranium series accessory crystal dating of magmatic processes. Annu. Rev. Earth Planet Sci. 39 https://doi.org/10.1146/annurev-earth-040610-133330.
Schmitt, A.K., Danišík, M., Evans, N., Siebel, W., Kiemele, E., Aydin, F., Harvey, J.C., 2011. Acigöl rhyolite field, Central Anatolia (part 1): high-resolution dating of eruption episodes and zircon growth rates. Contrib. Mineral. Petrol. 162 (6), 1233–1247.
Schmitt, A.K., Klitzke, M., Gerdes, A., Schäfer, C., 2017. Zircon hafnium–oxygen isotope and trace element petrochronology of intraplate volcanic rocks from the Eifel (Germany) and implications for mantle versus crustal origins of zircon megacrysts. J. Petrol. 58 (9), 1841–1870.
Schmitt, A.K., Martín, A., Stockli, D.F., Farley, K.A., Lovera, O.M., 2012. (U-Th)/He zircon and archaeological ages for a late prehistoric eruption in the Salton Trough (California, USA). Geology 41 (1), 7–10.
Schmitt, A.K., Stockli, D.F., Hausback, B.P., 2006. Eruption and magma crystallization ages of Las Tres Vírgenes (Baja California) constrained by combined $^{230}Th/^{238}U$ and (U-Th)/He dating of zircon. J. Volcanol. Geoth. Res. 158, 281–295.
Shane, P., Sandiford, A., 2003. Paleovegetation of marine isotope stages 4 and 3 in northern New Zealand and the age of the widespread Rotoehu tephra. Quat. Res. 59 (3), 420–429.
Shane, P., Nairn, I.A., Smith, V.C., 2005a. Magma mingling in the ~50 ka Rotoiti eruption from Okataina Volcanic Centre: implications for geochemical diversity and chronology of large volume rhyolites. J. Volcanol. Geoth. Res. 139, 295–313.
Shane, P.A.R., Smith, V.C., Nairn, I.A., 2005b. High temperature rhyodacites of the 36 ka Hauparu pyroclastic eruption, Okataina Volcanic Centre, New Zealand: change in a silicic magmatic system following caldera collapse. J. Volcanol. Geoth. Res. 147, 357–376.
Shane, P., Sikes, E.L., Guilderson, T.P., 2006. Tephra beds in deep-sea cores off northern New Zealand: implications for the history of Taupo Volcanic Zone, Mayor Island and White Island volcanoes. J. Volcanol. Geoth. Res. 154, 276–290.
Siddall, M., Rohling, E.J., Thompson, W.G., Waelbroeck, C., 2008. Marine isotope stage 3 sea level fluctuations: data synthesis and new outlook. Rev. Geophys. 46, RG4003.
Sisson, T.W., Schmitt, A.K., Danišík, M., Calvert, A.T., Pempena, N., Huang, C.Y., Shen, C.C., 2019. Age of the dacite of sunset amphitheater, a voluminous Pleistocene tephra from Mount Rainier (USA), and implications for Cascade glacial stratigraphy. J. Volcanol. Geoth. Res. 376, 27–43.
Smith, V., Shane, P., 2002. Geochemical characteristics of the widespread Tahuna tephra. N. Z. J. Geol. Geophys. 45, 103–107.
Smith, V.C., Shane, P., Smith, I.E.M., 2002. Tephrostratigraphy and geochemical fingerprinting of the Mangaone subgroup tephra beds, Okataina Volcanic Centre, New Zealand. N. Z. J. Geol. Geophys. 45 (2), 207–219.
Smith, V.C., Shane, P., Nairn, I.A., 2005. Trends in rhyolite geochemistry, mineralogy, and magma storage during the last 50 kyr at Okataina and Taupo volcanic centres, Taupo Volcanic Zone, New Zealand. J. Volcanol. Geoth. Res. 148 (3–4), 372–406.
Spencer, C.J., Kirkland, C.L., Taylor, R.J., 2016. Strategies towards statistically robust interpretations of in situ U–Pb zircon geochronology. Geoscience Frontiers 7 (4), 581–589.
Storm, S., Schmitt, A.K., Shane, P., Lindsay, J.M., 2014. Zircon trace element chemistry at sub-micrometer resolution for Tarawera volcano, New Zealand, and implications for rhyolite magma evolution. Contrib. Mineral. Petrol. 167 (4), 1000.

Storm, S., Shane, P., Schmitt, A.K., Lindsay, J.M., 2011. Contrasting punctuated zircon growth in two syn-erupted rhyolite magmas from Tarawera volcano: insights to crystal diversity in magmatic systems. Earth Planet Sci. Lett. 301 (3–4), 511–520.

Storm, S., Shane, P., Schmitt, A.K., Lindsay, J.M., 2012. Decoupled crystallization and eruption histories of the rhyolite magmatic system at Tarawera volcano revealed by zircon ages and growth rates. Contrib. Mineral. Petrol. 163 (3), 505–519.

Thompson, B.N., 1968. Age of Rotoiti breccia. N. Z. J. Geol. Geophys. 11 (5), 1189–1191.

Ulusoy, İ., Sarıkaya, M.A., Schmitt, A.K., Şen, E., Danišík, M., Gümüş, E., 2019. Volcanic eruption eye-witnessed and recorded by prehistoric humans. Quat. Sci. Rev. 212, 187–198.

Vandergoes, M.J., Hogg, A.G., Lowe, D.J., Newnham, R.M., Denton, G.H., Southon, J., Barrell, D.J.A., Wilson, C.J.N., McGlone, M.S., Allan, A.S.R., Almond, P.C., Petchey, F., Dabell, K., Dieffenbacher-Krall, A.C., Almond, P.C., 2013. A revised age for the Kawakawa/Oruanui tephra, a key marker for the Last Glacial Maximum in New Zealand. Quat. Sci. Rev. 74, 195–201.

Vermeesch, P., 2010. HelioPlot, and the treatment of overdispersed (U–Th–Sm)/He data. Chem. Geol. 271 (3–4), 108–111.

Vermeesch, P., 2012. On the visualisation of detrital age distributions. Chem. Geol. 312, 190–194.

Vermeesch, P., 2018. IsoplotR: a free and open toolbox for geochronology. Geoscience Frontiers 9 (5), 1479–1493.

Vucetich, C.G., Pullar, W.A., 1969. Stratigraphy and chronology of late Pleistocene volcanic ash beds in central North Island, New Zealand. N. Z. J. Geol. Geophys. 12 (4), 784–837.

Vucetich, C.G., Howorth, R., 1976. Late Pleistocene tephrostratigraphy in the Taupo district, New Zealand. N. Z. J. Geol. Geophys. 19, 51–69.

Wagner, G., Van den Haute, P., 2012. Fission-track Dating, vol. 6. Springer Science & Business Media.

Wiedenbeck, M.A.P.C., Alle, P., Corfu, F., Griffin, W.L., Meier, M., Oberli, F.V., von Quadt, A., Roddick, J.C., Spiegel, W., 1995. Three natural zircon standards for U-Th-Pb, Lu-Hf, trace element and REE analyses. Geostand. Newsl. 19 (1), 1–23.

Wilson, C.J.N., 2007. The geology of Mayor Island (Tuhua): a brief introduction. Geol. Soc. N. Z. Misc. Publ. 123B, 1–26.

Wilson, C.J., Rowland, J.V., 2016. The volcanic, magmatic and tectonic setting of the Taupo Volcanic Zone, New Zealand, reviewed from a geothermal perspective. Geothermics 59, 168–187.

Wilson, C.J.N., Houghton, B.F., Lanphere, M.A., Weaver, S.D., 1992. A new radiometric age estimate for the Rotoehu Ash from Mayor Island volcano, New Zealand. N. Z. J. Geol. Geophys. 35, 371–374.

Wilson, C.J.N., Rhoades, D.A., Lanphere, M.A., Calvert, A.T., Houghton, B.F., Weaver, S.D., Cole, J.W., 2007. A multiple-approach radiometric age estimate for the Rotoiti and Earthquake Flat eruptions, New Zealand, with implications for the MIS 4/3 boundary. Quat. Sci. Rev. 26, 1861–1870.

Wilson, C.J.N., Gravley, D.M., Leonard, G.S., Rowland, J.V., 2009. Volcanism in the central Taupo Volcanic Zone, New Zealand: tempo, styles and controls. In: Thordarson, T., Self, S., Larsen, G., Rowland, S.K., Hoskuldsson, A. (Eds.), "Studies in Volcanology: the Legacy of George Walker.". Special Publications of IAVCEI (Geological Society, London), 2, pp. 225–247.

Wright, I.C., McGlone, M.S., Nelson, C.S., Pillans, B.J., 1995. An integrated latest Quaternary (Stage 3 to present) paleoclimatic and paleooceanographic record from offshore northern New Zealand. Quat. Res. 44, 283–293.